https://doi.org/10.5194/egusphere-2023-3032
Preprint. Discussion started: 22 January 2024

Optimizing the terrestrial ecosystem gross primary productivity using carbonyl sulfide (COS) within a "two-leaf" modeling framework

Huajie Zhu[1‡], Xiuli Xing[1,2‡], Mousong Wu[1*], Weimin Ju[1], Fei Jiang[1,3]

1 International Institute for Earth System Science, Nanjing University, Nanjing, China

2 currently at: Department of Environmental Science and Engineering, Fudan University, Shanghai, China

3 Frontiers Science Center for Critical Earth Material Cycling, Nanjing University, Nanjing, China

Correspondence to: Mousong Wu (mousongwu@nju.edu.cn)

‡ they contribute equally to this work

Abstract. Accurately modeling gross primary productivity (GPP) is of great importance in diagnosing terrestrial carbon-climate feedbacks. Process-based terrestrial ecosystem models are often subject to substantial uncertainties, primarily attributed to inadequately calibrated parameters. Recent attention has identified carbonyl sulfide (COS) as a promising proxy of GPP, due to the close linkage between leaf exchange of COS and carbon dioxide (CO_2) through their shared pathway of stomatal diffusion. However, most of the current modeling approaches for COS and CO_2 did not explicitly consider the vegetation structural impacts, i.e. the differences between the sun-shade and sunlit leaves in COS uptake. This study used ecosystem COS fluxes data from 7 sites to optimize GPP estimation across various ecosystems with the Boreal Ecosystem Productivity Simulator (BEPS), which was further developed for simulating the leaf COS uptake under its state-of-the-art 'two-leaf' framework. Our results demonstrated the substantial improvement in GPP simulation across various ecosystems through the fusion of COS data into the 'two-leaf' model, with the ensemble mean of root mean square error (RMSE) for simulated GPP reduced by 18.99 % to 66.64 %. Notably, we also shed light on the remarkable identifiability of key parameters within the BEPS model, including the maximum carboxylation rate of Rubisco at 25 ℃ (V_{cmax25}), minimum stomatal conductance (b_{H_2O}), and leaf nitrogen content (N_{leaf}), despite intricate interactions among COS-related parameters. Furthermore, our global sensitivity analysis delineated both shared and disparate sensitivities of COS and GPP to model parameters and suggested the unique treatment of parameters for each site in COS and GPP modeling. In summary, our study deepened insights into the sensitivity, identifiability, and interactions of parameters related to COS, and showcased the efficacy of COS in reducing uncertainty in GPP simulations.

Keywords: carbonyl sulfide, photosynthesis, model-data fusion, ecosystem modeling, parameter optimization

https://doi.org/10.5194/egusphere-2023-3032
Preprint. Discussion started: 22 January 2024

1 Introduction

Over the past five decades, terrestrial ecosystems have been absorbing about 30 % of anthropogenic carbon dioxide (CO_2) emissions, playing a crucial role in mitigating climate change (Friedlingstein et al., 2022). Driven by the photosynthesis of terrestrial vegetation, the gross primary productivity (GPP), is the largest terrestrial carbon flux and plays an important role in understanding terrestrial carbon-climate feedbacks (Luo, 2007; Wang et al., 2021). However, as the direct observations of GPP using atmospheric CO_2 observations are confounded by respiration (Hilton et al., 2017), and the modeling of GPP are affected by a range of uncertainties, such as the poorly calibrated parameters (Macbean et al., 2022), the precise quantification of GPP in terrestrial ecosystems has been a major challenge (Canadell et al., 2000; Yuan et al., 2007).

In the past decade, carbonyl sulfide (COS) has emerged as a promising tracer for terrestrial photosynthesis (Stimler et al., 2010; Asaf et al., 2013; Billesbach et al., 2014; Maseyk et al., 2014; Launois et al., 2015; Hilton et al., 2017; Yang et al., 2018; Kooijmans et al., 2019; Spielmann et al., 2019; Hu et al., 2021; Kohonen et al., 2022) and stomatal conductance (Commane et al., 2015; Wehr et al., 2017; Sun et al., 2022; Cho et al., 2023) as the leaf exchange of COS and carbon dioxide (CO_2) are tightly coupled through stomata (Goldan et al., 1988; Sandoval-Soto et al., 2005; Seibt et al., 2010; Wohlfahrt et al., 2012; Whelan et al., 2018). Unlike CO_2, which is emitted back to the atmosphere via leaf respiration (Sun et al., 2022), COS is completely destroyed by a hydrolysis reaction catalyzed by carbonic anhydrase (Protoschill-Krebs et al., 1996) without back-flux in leaves under normal conditions (Stimler et al., 2010). Consequently, the measurement of COS flux is able to provide a direct and independent way to estimate GPP (Sandoval-Soto et al., 2005; Abadie et al., 2023).

In most of the early studies, GPP was directly estimated by scaling measurement of plant COS uptake with the empirically derived leaf relative uptake (LRU) or its extensions that take the effects of humidity, light and CO_2 concentration on stomatal conductance into account (Kohonen et al., 2022; Sun et al., 2022; Abadie et al., 2023) because of the simplicity of this approach and the sufficiency of it in many cases (Sandoval-Soto et al., 2005; Whelan et al., 2018). In contrast, the process-based model that mechanistically simulates COS plant uptake by incorporating stomatal transport processes were also developed and widely evaluated (Maignan et al., 2021; Kooijmans et al., 2021). Concurrently, the significance of soil COS exchange has also been recognized, leading to the development of a suite of empirical or mechanistic COS soil exchange models (Kesselmeier et al., 1999; Berry et al., 2013; Launois et al., 2015; Sun et al., 2015; Ogée et al., 2016; Whelan et al., 2022). Process-based COS plant uptake model and soil exchange model have been integrated into land surface models (LSMs) (Berry et al., 2013; Maignan et al., 2021; Kooijmans et al., 2021; Chen et al., 2023). Consequently, by constraining the model parameters of LSMs with COS through data assimilation, not only the model variables like GPP are expected to be optimized, but also our understanding of ecosystem processes is expected to be significantly deepened.

Currently, several studies have been endeavored to refine the model parameters of LSMs through assimilating the COS data, and thereby optimized the modeling of water-carbon fluxes (Chen et al., 2023; Abadie et al., 2023). Abadie et al. (2023) demonstrated COS could provide mechanistic constraint on stomatal diffusion, and the joint assimilation of COS and GPP can also improve the model performance of GPP and latent heat. Ecosystem carbon, water and energy processes are interacted and

https://doi.org/10.5194/egusphere-2023-3032
Preprint. Discussion started: 22 January 2024

nonlinear, the changes in one process could induce variations in the other processes. While COS assimilation has proven effective in constraining COS-related model parameters and optimizing GPP, there remains a gap of systematic understanding of the ability of COS to optimize model parameters from different processes, e.g. how effective is the assimilation of COS in reducing model prediction uncertainty of GPP as well as the relevant ecosystem processes in different ecosystems?

In this context, we have further explored the capacity of COS to constrain the model parameters of LSM and to optimize GPP, with the aims to answering the following questions:

Which parameters the COS simulation is sensitive to, and what are the differences in parameter sensitivities between COS and GPP?

How effective is COS assimilation in enhancing model prediction and reducing prediction uncertainty of GPP?

Which process parameters can be well identified by the assimilation of COS?

How do process parameters interact in COS modeling across diverse ecosystems?

To address these questions, we utilized the ecosystem COS flux data to optimize GPP across various ecosystems based on the combination of COS modeling with the Boreal Ecosystem Productivity Simulator (BEPS). Specifically, we investigated the usefulness of COS in constraining the ecosystem processes related to not only photosynthesis, but also the water and energy. Furthermore, parameter uncertainties as well as the uncertainties in the optimization results were evaluated.

2 Materials and methods

2.1 Model description

2.1.1 BEPS basic model

The BEPS model (Liu et al., 1997; Chen et al., 1999; Chen et al., 2012) used in this study is a process-based diagnostic model driven by remotely sensed vegetation parameters, including LAI, clumping index, and land cover type, as well as meteorological and soil data (Chen et al., 2019). With the consideration of coupling among terrestrial carbon, water, and nitrogen cycles (He et al., 2021), it simulates photosynthesis, energy balance, and hydrological and soil biogeochemical processes at hourly time steps (Ju et al., 2006; Liu et al., 2015). For photosynthesis, it stratifies whole canopies into sunlit and shaded leaves and calculated GPP for each group of leaves by scaling Farquhar's leaf biochemical model (Farquhar et al., 1980) up to canopy-level with a temporal and spatial scaling scheme (Chen et al., 1999). In this study, the BEPS model stratifies the soil profile into five layers, and the model implicitly solves the soil water content values for these layers (Ju et al., 2010). Over the last few decades, the BEPS model has been continuously improved and has been used in a wide variety of terrestrial ecosystems (Schwalm et al., 2010; Liu et al., 2015). This study used the BEPS model that simulates water, carbon and energy processes at hourly interval which enables the detection of diel variations of model variables (Xing et al., 2023).

https://doi.org/10.5194/egusphere-2023-3032
Preprint. Discussion started: 22 January 2024

2.1.2 The 'two-leaf' scheme for GPP and COS modeling

The BEPS model simulates the canopy photosynthesis for the sunlit and sun-shade leaves separately,

$$\mathrm{GPP} = GPP_{sunlit} LAI_{sunlit} + GPP_{shaded} LAI_{shaded} \quad (1)$$

where GPP_{sunlit} and GPP_{shaded} denote the GPP per unit area for sunlit and shaded leaves, LAI_{sunlit} and LAI_{shaded} represent the LAI values of sunlit and shaded leaves, respectively. The detailed descriptions about the photosynthesis modeling approach of BEPS are illustrated in Appendix A1.

The ecosystem COS flux includes both plant COS uptake $F_{cos,plant}$ and soil COS flux exchange $F_{cos,soil}$ (Whelan et al., 2016). In this work, the canopy-level COS plant uptake $F_{cos,plant}$ (pmol m^{-2} s^{-1}) was calculated by upscaling the resistance analog model of COS uptake (Berry et al., 2013) with the 'two-leaf' upscaling scheme (Chen et al., 1999). Considering the different responses of foliage to diffuse and direct solar radiation (Gu et al., 2002), $F_{cos,plant}$ is calculated as:

$$F_{cos,plant} = F_{cos,sunlit} LAI_{sunlit} + F_{cos,shaded} LAI_{shaded} \quad (2)$$

where $F_{cos,sunlit}$ and $F_{cos,shaded}$ denote the leaf-level COS uptake rate (pmol m^{-2} s^{-1}) for sunlit and shaded leaves.

The soil COS fluxes are simulated by considering the abiotic and biotic components separately, as by Whelan et al. (2016). We took the soil COS modeling scheme including the parameterizations from Abadie et al. (2022) and Whelan et al. (2022) in this study (see Appendix A2) given that our focus is the COS and GPP relationships and the previous studies have verified this approach over multiple sites with measurements.

2.2 Site description

The model was evaluated on seven sites distributed on the Eurasian and American continents in boreal, temperate and subtropical regions based on field observations collected from several studies. Those sites were representative of different climate regions and land cover types (in the model represented by plant function types, and soil textures, as depicted in **Table 1**).

Table 1. Site characteristics. Site identification includes the country initials and a three-letter name for each site. locations of the sites are provided by the latitude (Lat) and longitude (Lon). PFT stands for plant functional type. ENF and DBF denote evergreen needleleaf forest and deciduous broadleaf forest respectively.

Site name	Lat (°N)	Lon (°E)	PFT	Soil texture	Year	References
AT-Neu	47.12	11.32	Grass	Silty clay loam	2015	Spielmann et al. (2019)
DK-Sor	55.49	11.64	DBF	Silty clay	2016	Spielmann et al. (2019)
ES-Lma	39.94	-5.77	Grass	Silty clay	2016	Spielmann et al. (2019)
FI-Hyy	61.85	24.29	ENF	Loamy sand	2013-2017	Vesala et al. (2022)
IT-Soy	45.87	13.08	Crop	Silty clay loam	2017	Spielmann et al. (2019)
US-Ha1	42.54	-72.17	DBF	Loam	2012-2013	Wehr et al. (2017)
US-Wrc	45.82	-121.95	ENF	Silty loam	2014	Rastogi et al. (2018)

https://doi.org/10.5194/egusphere-2023-3032
Preprint. Discussion started: 22 January 2024

2.3 Data

2.3.1 LAI dataset

The satellite LAI data that best matched the field measurements was selected from three candidate LAI products to drive the model. The LAI dataset used here are the GLOBMAP global leaf area index product (Version 3) (see GLOBMAP global Leaf Area Index since 1981 | Zenodo) and the Global Land Surface Satellite (GLASS) LAI product (Version 3) (acquired from ftp://ftp.glcf.umd.edu/). They represent Leaf area index at a spatial resolution of 8 km (Liu et al., 2012) and 1 km (Xiao et al., 2016) respectively, and a temporal resolution of 8-day. With reference to the observed LAI at these sites (Wehr et al., 2017; Rastogi et al., 2018; Spielmann et al., 2019; Kohonen et al., 2022), the GLASS LAI was adopted to DK-Sor and IT-Soy, and the GLOBMAP LAI was utilized for the remaining five sites. In addition, these LAI products were interpolated into daily values by the nearest neighbor method for the simulation.

2.3.2 Meteorological dataset

Meteorological data required to force the BEPS model include air temperature, shortwave radiation, precipitation, relative humidity and wind speed. As the simulations were conducted at the site scale, we utilized the FLUXNET2015 data (see https://fluxnet.org for AT-Neu, DK-Sor and ES-Lma and FI-Hyy) and the AmeriFlux data (see https://ameriflux.lbl.gov for US-Ha1 and US-Wrc). Specifically, as FLUXNET2015 meteorological data for AT-Neu were only accessible for the period 2002-2012, we conducted a linear fit between its ERA5 data (https://cds.climate.copernicus.eu/cdsapp#!/dataset/reanalysis-era5-single-levels?tab=overview) and FLUXNET2015 meteorological data for the corresponding period. Then, we used the fitted parameters to adjust the ERA5 data for 2015, thereby obtaining downscaling information for the meteorological data. In addition, the shortwave radiation data of US-Ha1 were derived from ERA5 due to the lack of available data in AmeriFlux.

2.3.3 COS and GPP datasets

The hourly ecosystem COS flux observations were utilized to perform optimization and to evaluate the optimization results. They were derived from existing studies with pre-processing with regard to the data quality check, as listed in **Table1**. To assess the model performance of GPP, the GPP observations were also collected from FLUXNET (DK-Sor, ES-Lma and FI-Hyy), AmeriFlux (US-Ha1 and US-Wrc), and Spielmann et al. (2019) (AT-Neu and IT-Soy). Given that only CO_2 turbulent flux (FC) or net ecosystem exchange (NEE) data were available at AT-Neu, IT-Soy, US-Ha1 and US-Wrc, a night flux partitioning model (Reichstein et al., 2005) was employed to derive GPP. This model assumes that nighttime NEE represents ecosystem respiration R_{eco}, and thus partitions FC or NEE into GPP and R_{eco} based on the semi-empirical models of respiration, which use air temperature as a driver (Lloyd and Taylor, 1994; Lasslop et al., 2012).

https://doi.org/10.5194/egusphere-2023-3032
Preprint. Discussion started: 22 January 2024

2.4 The Monte Carlo-based parameter calibration

To evaluate the sensitivity, equifinality and interaction of model parameters, and the uncertainty of model outputs, the Monte Carlo-based parameter calibration methodology was employed here. The methodology calls for rejecting the concept of a unique global optimum parameter set within some particular model structure, instead recognizing the "equifinality" of parameter sets that exhibit similarly good performance in producing the observed data (Beven and Freer, 2001). Thus, the result is depicted with an ensemble of acceptable or behavioral parameter sets conditioned on the available observational data (Blasone et al., 2008; Beven and Binley, 2014). This method has been extensively used in ecosystem modeling with multiple parameters to be calibrated and shown high ability in constraining multiple ecosystem processes (Tonkin and Doherty, 2009; Houska et al., 2014; He et al., 2016; Wu et al., 2019; Wu et al., 2020; Xing et al., 2023).

2.4.1 Parameter selection and sampling strategy

Based on current understanding of COS exchange (Wohlfahrt et al., 2012; Berry et al., 2013; Whelan et al., 2016; Whelan et al., 2018; Cho et al., 2023) and photosynthesis processes (Ball et al., 1987; Raines, 2003; Blankenship, 2021) and related parameter sensitivity studies (Liu et al., 2011; Chen et al., 2012; Chen et al., 2023; Xing et al., 2023), 9 parameters were selected to be calibrated in this study (for details see **Table B1**). These parameters are related to formulas describing four processes: 1) photosynthesis (V_{cmax25}, VJ_{slope}, N_{leaf}), 2) soil hydrology ($Ksat_{scalar}$, b_{scalar}, r_{decay}), 3) stomatal gas exchange (b_{H_2O}, m_{H_2O}), and 4) energy balance (f_{leaf}). Specifically, $Ksat_{scalar}$ and b_{scalar} are scaling factors designed to optimize the saturated hydraulic conductivity (Ksat) and the Campbell parameter (b) for each soil layer in the BEPS model. The default values and prior ranges for these parameters (**Table B1**) were chosen based on literature and default model settings. Uniform distributions were assigned to all parameters, and 20,000 sets of parameters were generated through random sampling.

2.4.2 Selection of behavioral simulations

To measure the agreement between model simulations and observations, a variety of performance metrics have been proposed and utilized in in previous studies (Beven and Binley, 1992; Moradkhani et al., 2005; Staudt et al., 2010). In this study, we employed the root mean square error (RMSE) to distinguish between behavioral and non-behavioral simulations.

$$RMSE = \sqrt{\frac{1}{N}\sum_{i=1}^{N}(obs_i - sim_i)^2} \quad (3)$$

where N is the total number of observations."obs" and "sim" denote the observations and simulations, respectively. sim_i denotes the simulation corresponding to the *i* th observation obs_i.

In specific, we chose the top 0.5 % runs with the lowest RMSE values for COS as behavioral simulations. Thus, the deterministic model prediction is given by the ensemble mean of the 100 behavioral simulations.

https://doi.org/10.5194/egusphere-2023-3032
Preprint. Discussion started: 22 January 2024

2.4.3 Uncertainty quantification

The model prediction limits or uncertainty bounds can be determined by forming the cumulative density function (CDF) of the ensemble of simulations (Beven and Binley, 2014), normally chosen at the 5 % and 95 % confidence level in most of the previous studies (Blasone et al., 2008). Similarly, we chose the 5 % and 95 % quantiles of the 20,000 simulations and the behavioral simulations to quantify the model output uncertainty in this study.

2.5 Parameter sensitivity

In order to take full advantage of Monte Carlo sampled parameter sets, a density-based global sensitivity analysis approach (Plischke et al., 2013) was used to investigate the sensitivity of COS and GPP simulations to the selected model parameters via the Sensitivity Analysis Library (SALib) (Iwanaga et al., 2022). This approach aims at assessing the influence of the entire input distribution on the entire output distribution without reference to a particular moment of the output (Borgonovo, 2007). According to Borgonovo (2007), the sensitivity index (δ) is always between 0 and 1, it equals 0 if the output is not dependent upon the model parameter, and it equals unity if all model parameters is considered.

2.6 Parameter uncertainty

Due to the complexity of ecosystem, ecosystem models often require a substantial number of parameters to realize the modeling of various ecosystem processes, and some parameters are compensating with each other (Mo et al., 2008). While the parameter interactions related to photosynthesis have been systematically studied (Tang and Zhuang, 2009; Lu et al., 2013; Wu et al., 2019; Xing et al., 2023), the parameter interactions related to COS flux simulation have not been reported. Based on the Monte Carlo-based methodology, the numerous behavioral parameter sets around the "optimum" (Beven and Freer, 2001) provide us with the opportunity to analyze the interactions between the selected parameters. In this study, the Pearson correlation coefficient and the confidence level were employed to identify the parameter interactions.

Parameter identifiability (PI) is the concept of whether uncertain parameters can be correctly estimated from the observed data (Yi et al., 2019). The failure in PI is supposed to be caused by 'over-parameterization" and parameter interactions (due to high nonlinearity of model equations) (Gan et al., 2014). Inspired by Yi et al. (2019) who used likelihood confidence interval as a measure of PI, here we used parameter distribution range for the same purpose. Taking into account the influence of the prior distribution to the behavioral parameter sets, the PI is defined as the reduction of the parameter range width. Hence, a large value of PI indicates that the parameter is well identified in the calibration process.

https://doi.org/10.5194/egusphere-2023-3032
Preprint. Discussion started: 22 January 2024

3 Results

3.1 Parameter sensitivity

The sensitivity indexes of COS and GPP simulations to the model parameters for the seven sites are illustrated in **Fig. 1**. It can be seen that both COS and GPP simulations exhibit high sensitivity to leaf nitrogen content (N_{leaf}) and the maximum carboxylation rate of Rubisco at 25 °C (V_{cmax25}), while showing low sensitivity to soil hydrology related parameters, including b_{scalar}, $Ksat_{scalar}$ and r_{decay}. With the average values of sensitivity index of 0.14, 0.12 and 0.08, the photosynthesis related parameters f_{leaf} and VJ_{slope} as well as stomata conductance related parameter m_{H_2o} can significantly impact the simulation of GPP. However, those parameters do not exhibit high sensitivity in the modeling of COS. Furthermore, our results highlight the crucial role of the intercept of the Ball-Berry model (b_{H_2o}) in the modeling of COS, yet its impact on the simulation of GPP is limited. In summary, our results suggest that the simulated COS and GPP share some similarities in their sensitivities to parameters, but there are also notable differences. Specifically, parameters including f_{leaf}, m_{H_2o} and VJ_{slope} strongly influence GPP modeling but have minimal impacts on COS modeling.

With the mean values of 0.30, 0.29 and 0.09 respectively, the sensitivity indexes of COS simulations to V_{cmax25}, N_{leaf} and b_{H_2o} are much larger than those of GPP simulations. However, the patterns of the sensitivity of these parameters for COS and GPP simulations are very similar at these sites. Specifically, our results reveal that the simulated COS and GPP are more sensitive to N_{leaf}, while less sensitive to V_{cmax25} at evergreen needleleaf forest sites (FI-Hyy and US-Wrc). In contrast, at the crop site (IT-Soy), V_{cmax25} plays a more crucial role in the simulation of COS and GPP, whereas N_{leaf} does the opposite. We also found that m_{H_2o} is much more important in the modeling of GPP at US-Wrc than other sites and f_{leaf} has a smaller effect on GPP simulations in the savanna site (ES-Lma). Furthermore, our results suggest that the modeling of GPP at deciduous broadleaf forest sites (DK-Sor and US-Ha1) are more sensitive to VJ_{slope} while less sensitive to m_{H_2o} than at other sites.

https://doi.org/10.5194/egusphere-2023-3032
Preprint. Discussion started: 22 January 2024

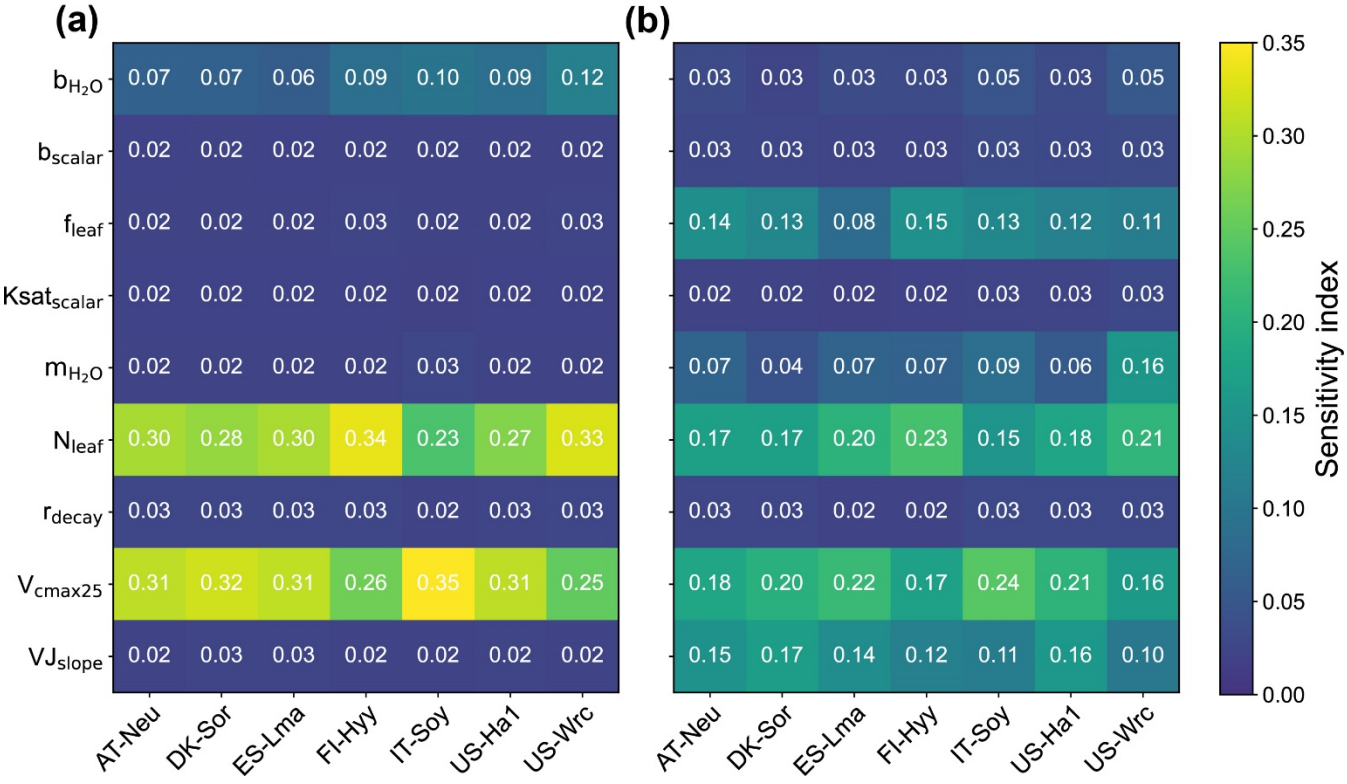

Figure 1. Sensitivity indexes of the modelled ecosystem COS fluxes (**a**) and GPP (**b**) to model parameters.

3.2 Posterior parameter distributions

The cumulative frequency distribution as well as the boxplots of each of the parameters for the 0.5 % best runs were plotted in **Fig. 1**, with a comparison to the uniform parameter distributions and the default parameters. As shown in **Fig. 1**, the posterior distributions of these parameters differ significantly, indicating that the response of these parameters to the assimilation of COS is quite different. Our results demonstrated that COS fluxes have similar constraining effects to the same parameters in different ecosystems although the posterior distributions of the same parameter at different sites depicted variations. In general, parameters related to plant growth and stomatal conductance were strongly constrained by the assimilation of COS, while the parameters related energy balance as well as soil hydrology were inadequately constrained.

With distinct shape and remarkably narrow range of the cumulative frequency curves, b_{H_2o} (the intercept of the Ball-Berry model, representing minimum stomatal conductance) was strongly constraint by the assimilation of COS in this study. For most sites (AT-Neu, FI-Hyy, IT-Soy and US-Ha1), the values of b_{H_2o} were confined to a very limited range of 0 to 0.09 mol m^{-2} s^{-1}, with the average value of the posterior b_{H_2o} less than 0.04 mol m^{-2} s^{-1}. For DK-Sor and ES-Lma, the posterior range width of b_{H_2o} are much larger, with values of 0.39 mol m^{-2} s^{-1} and 0.26 mol m^{-2} s^{-1} respectively. With posterior b_{H_2o} values ranging from 0.21 to 0.99 mol m^{-2} s^{-1}, US-Wrc is the only site where the default value of b_{H_2o} (0.0175

https://doi.org/10.5194/egusphere-2023-3032
Preprint. Discussion started: 22 January 2024

mol m^{-2} s^{-1}) for the BEPS model was rejected by the assimilation of COS. Despite the broad distribution of posterior b_{H_2O} at US-Wrc, the cumulative frequency curve still indicates that b_{H_2O} is well-constrained at this site, with 85 % of the posterior b_{H_2O} located in a narrow range of 0.21 to 0.50 mol m^{-2} s^{-1}. Overall, our results are reasonable as literature-documented values of b_{H_2O} are highly variable and they align well with the compilation provided by Miner et al. (2017), in which more than 83 % of the b_{H_2O} values are located between 0 and 0.15 mol m^{-2} s^{-1}, and about half are located between 0 and 0.04 mol m^{-2} s^{-1}. Moreover, the mean values of posterior b_{H_2O} for all sites are larger than the default b_{H_2O} value of the BEPS model, suggesting that the current b_{H_2O} value utilized in BEPS may be underestimated.

Identified as the most sensitive parameters in COS modeling, the plant growth related parameter V_{cmax25} and N_{leaf} were generally well constrained in this study. However, unlike b_{H_2O}, which is strongly constrained at all sites, the posterior cumulative frequency curves of V_{cmax25} and N_{leaf} exhibit considerable variation across sites. Except for the evergreen needleleaf forest sites US-Wrc, the posterior V_{cmax25} and N_{leaf} were mostly distributed in the upper half of the parameter range. Particularly, all of the lower half values of V_{cmax25} and N_{leaf} were excluded by the behavioral parameter sets at DK-Sor and ES-Lma. In contrast, at FI-Hyy, both the posterior cumulative frequency curves of V_{cmax25} and N_{leaf} deviated slightly from the original uniform distribution, indicating that they are not well-constrained by the assimilation of COS. Notably, the assimilation of COS effectively excluded the upper half values of N_{leaf} in US-Wrc, while not for V_{cmax25}.

Another stomatal conductance-related parameter, m_{H_2O}, demonstrated effective constraint through COS assimilation at specific sites (DK-Sor, ES-Lma, FI-Hyy, and IT-Soy), with parameter range width reductions comparable to V_{cmax25} and N_{leaf}. However, at the remaining sites, the posterior cumulative frequency curves of m_{H_2O} show minimal deviation from the original uniform distribution. Nevertheless, the optimization of m_{H_2O} is generally achievable through COS assimilation, as supported by our results in good agreement with the compilation of Miner et al. (2017). As indicated in **Table 2**, the average absolute bias between the default m_{H_2O} and the grouping value reached as high as 2.87 for these sites. Through COS assimilation, the mean absolute bias was reduced to 2.43. In particular, the disparities between the mean posterior m_{H_2O} and the grouping value are consistently smaller than those between the default value and the grouping value, with the exception of DK-Sor and US-Wrc. However, it is noteworthy that our optimization results for DK-Sor and US-Wrc remain plausible, as they fall within one standard deviation (SD) of the grouping values.

Table 2. Mean posterior m_{H_2O} values for seven study sites in comparison with the default values and the PFT grouping values (mean ± standard deviation) (Miner et al., 2017). Within the compilation of Miner et al. (2017), FI-Hyy and US-Wrc are classified under the PFT of evergreen gymnosperm tree, while DK-Sor and US-Ha1 fall under the PFT of deciduous angiosperm tree.

Site name	AT-Neu	DK-Sor	ES-Lma	FI-Hyy	IT-Soy	US-Ha1	US-Wrc
default	8	8	8	8	8	8	8
This study	8.26	11.46	10.69	5.89	9.63	8.65	8.55
Miner 2017	13.3 ± 3.1	8.7 ± 5.1	13.3 ± 3.1	6.7 ± 2.5	13.5 ± 3.1	8.7 ± 5.1	6.7 ± 2.5

https://doi.org/10.5194/egusphere-2023-3032
Preprint. Discussion started: 22 January 2024

The photosynthesis-related parameters VJ_{slope} and f_{leaf} also influence COS simulation. In behavioral parameter sets for DK-Sor and ES-Lma, excessively small values (less than 0.2) for f_{leaf} were effectively rejected. However, the posterior distributions of f_{leaf} resemble the original uniform distribution, suggesting that it is not a crucial parameter for COS simulations. The posterior cumulative frequency curve of VJ_{slope} also deviates slightly from the uniform distribution. Yet, at DK-Sor, more than three-quarters of the posterior VJ_{slope} values are situated in the upper half of the parameter range, indicating that VJ_{slope} can also be well-constrained by the assimilation of COS in specific cases.

Among these seven sites, the soil hydrology-related parameters $Ksat_{scalar}$, b_{scalar},, and r_{decay} did not exhibit a strong response during the assimilation of COS. However, the posterior cumulative frequency curves of these parameters show notable deviations from the uniform distribution in certain cases. Specifically, at FI-Hyy, higher values of b_{scalar}, $Ksat_{scalar}$, and r_{decay} are more prevalent within the behavioral parameter sets, leading to posterior means for these parameters that are all greater than the prior means.

https://doi.org/10.5194/egusphere-2023-3032
Preprint. Discussion started: 22 January 2024

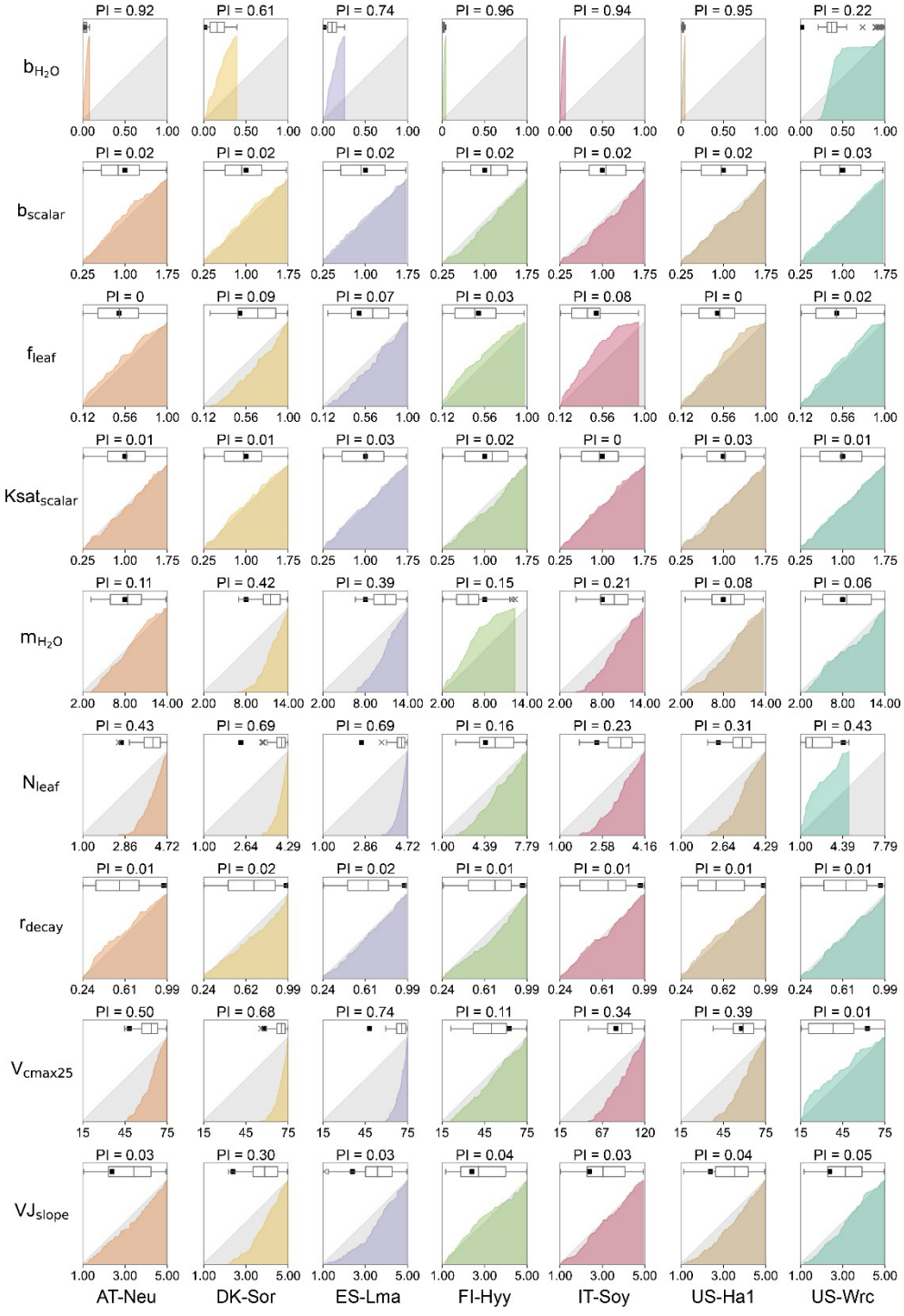

Figure 2. Cumulative frequency distributions and boxplots for the posterior model parameters. The grey area represents a uniform parameter distribution and the black square represents the default parameter value.

https://doi.org/10.5194/egusphere-2023-3032
Preprint. Discussion started: 22 January 2024

3.3 The optimization performance in COS fluxes

The posterior simulated COS fluxes were evaluated against the prior simulations and observations. **Table 3** lists the mean RMSEs and range widths of the prior and posterior simulated COS fluxes for all the sites. The $RMSE_{mean}$ of the posterior COS simulations are smaller than the prior, and the mean RMSE reduction for all sites is 32.09 % ± 13.49 % (mean ± SD). At the same time, the simulation range widths of COS fluxes are also well constrained, with a mean reduction of 76.42 % ± 13.31 % from the prior. The reduction of $RMSE_{mean}$ and range width is particularly significant in US-Wrc, with a value of 61.39 % and 96.77 %, respectively.

In **Fig. 2**, the daily and monthly variations of COS during the observation period at each site are shown. It can be observed that both the prior and posterior simulations are able to accurately capture the daily variation or the seasonal cycle of COS across these sites, with the exception of IT-Soy. As IT-Soy is a temporary observatory with no continuous in-situ meteorological observations available, the ERA-5 meteorological data were used to drive the model for this site, resulting in the simulation not being able to characterize the COS changes very well. Although the simulations perform well in modeling the variations of COS for other sites, our results also suggest that they tend to underestimate the magnitude of COS fluxes at both ends of the growing season (e.g. **Fig. 2d**). Furthermore, the model markedly underestimates the magnitude of COS during rainy days (DOY 126-134) at ES-Lma (**Fig. 3c**). These findings suggest substantial deficiencies in modeling the mechanistic process of COS exchange. Nevertheless, it can be stated that the fusion of COS observations with the BEPS model has the capacity in constraining the predictive uncertainty of COS, as evidenced by significantly reduced uncertainty bounds that largely encapsulate observations.

The prior simulations tend to underestimate the COS fluxes at DK-Sor and ES-Lma, with the ensemble mean of prior simulations being only about half that of the observations. After calibration, the simulated COS fluxes show a substantial increase and generally align with the observations. However, some observed peaks are still not included in the posterior simulation uncertainty bounds. In contrast, the prior simulations tend to overestimate COS fluxes at the evergreen needleleaf forest sites, especially US-Wrc, where the ensemble mean of prior simulations are 78.43 % larger than the observations. The assimilation of COS also effectively corrected the overestimation but, at the same time, led to a further underestimate of the magnitude of variation in the simulated COS for US-Wrc. In addition, with the down-regulation of COS simulations, the model-observation difference at both ends of the growing season for FI-Hyy further increased. Particularly, significant underestimation is found in the posterior simulations in 2017 for FI-Hyy, despite remarkable improvement is attached by the posterior simulations in reproducing COS fluxes over the entire period (2013-2017). As the prior simulations neither noticeably overestimate nor underestimate, there is little difference between the ensemble mean of the prior and posterior simulations at the remaining three sites (AT-Neu, IT-Soy and US-Ha1). Nevertheless, the assimilation of COS resulted in a remarkable reduction in both $RMSE_{mean}$ and uncertainty bounds for COS simulations at these sites, with mean reductions of 24.25 % and 79.43 %, respectively.

https://doi.org/10.5194/egusphere-2023-3032
Preprint. Discussion started: 22 January 2024

Overall, there are considerable uncertainties in the prior simulations, with the uncertainty bounds comparable to or much larger than the uncertainties of observations, and the ensemble mean deviate remarkable from observations in some sites, i.e., DK-Sor. Our results suggest that significant improvement in both the ensemble mean and predictive uncertainty of COS simulations can be achieved through the addition of the information provided by the COS observations with the Monte Carlo-based parameter calibration, especially for evergreen needleleaf forest sites. However, limited by various factors, such as uncertainty in model-driven data and model structure (Cho et al., 2023), currently the model often underestimates the simulation at both ends of the growing season, and lacks proficiency in modeling the magnitude of COS during rainy days.

Table 3. Comparison of model performance indices for the prior and posterior COS simulations. The $RMSE_{mean}$ of the prior and posterior simulations are the mean values of the RMSEs of 20,000 prior COS simulations and 100 behavioral COS simulations with COS observations, respectively. The range widths of the prior and posterior COS simulations are defined as the mean values of the difference between the 95th and 5th percentile of the prior and posterior simulations, respectively.

Site name	$RMSE_{mean}$ (pmol m^{-2} s^{-1})			Range width (pmol m^{-2} s^{-1})		
	Prior	Posterior	Reduction (%)	Prior	Posterior	Reduction (%)
AT-Neu	16.01	11.69	27.01	22.79	5.59	75.45
DK-Sor	32.03	22.09	31.04	23.85	10.54	55.81
ES-Lma	12.96	10.42	19.62	6.85	2.76	59.68
FI-Hyy	17.35	10.43	39.84	35.85	5.59	84.40
IT-Soy	16.84	13.22	21.53	22.58	4.60	79.61
US-Ha1	20.24	15.34	24.22	43.88	7.35	83.24
US-Wrc	36.12	13.95	61.39	70.17	2.27	96.77

https://doi.org/10.5194/egusphere-2023-3032
Preprint. Discussion started: 22 January 2024

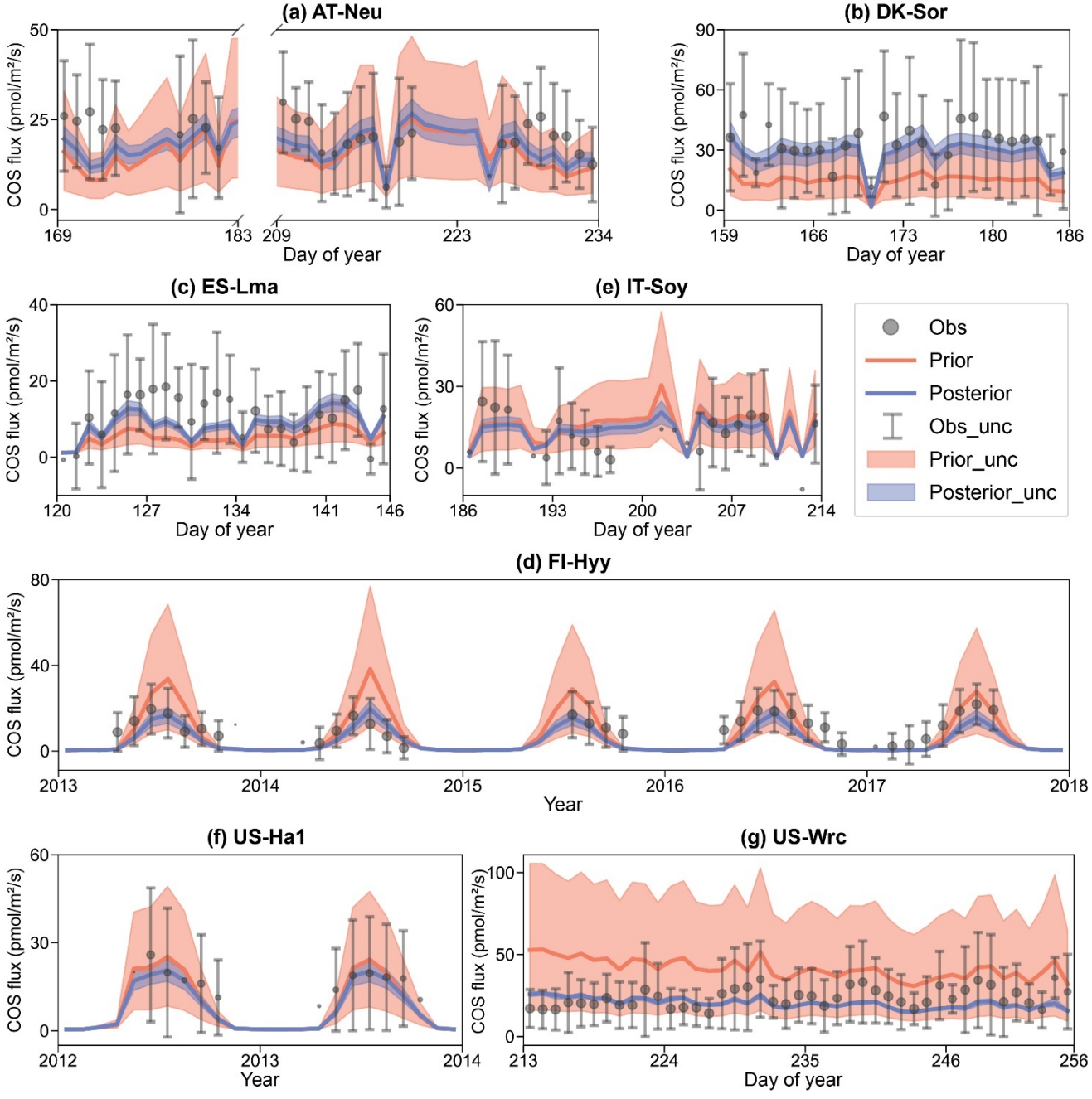

320 **Figure 3.** Comparison of prior and posterior simulated ecosystem COS fluxes. The ensemble means of the prior (red) and posterior (green) simulations are plotted around the uncertainty bounds (5th and 95th quantile). The mean observed COS and its uncertainty (± 1 standard deviation) are represented by blue dots with error bars. The means and uncertainties of these observations and simulations are calculated and plotted on a daily or monthly scale. Particularly, error bars are not plotted when more than 3/4 of the observations are missing.

https://doi.org/10.5194/egusphere-2023-3032
Preprint. Discussion started: 22 January 2024

3.4 The performance of simulated GPP

The mean RMSEs and range widths of both prior and posterior simulated GPP for all sites are presented in **Table 4**. With reduction ratios of $RMSE_{mean}$ ranging from 18.99 % to 66.64 %, the assimilation of COS effectively enhanced the model performance of GPP to varying degrees. Concurrently, the range widths of GPP simulations were well confined, exhibiting a mean reduction ratio of 51.83 % ± 17.02 %. Notably, the maximum reduction in both $RMSE_{mean}$ and range width for GPP occurred at US-Wrc, aligning with the substantial improvement observed in the posterior simulated COS at this site. In contrast, a relatively limited impact on improving the prediction of GPP was observed at AT-Neu, as evidenced by both the smaller reduction in $RMSE_{mean}$ and range width of GPP simulations.

The BEPS model demonstrated excellent performance in capturing the daily variation and seasonal cycle of GPP, as illustrated in **Fig. 3**. However, similar to the COS simulations, the ensemble averages of the prior simulated GPP notably deviated from observations at several sites. Specifically, at DK-Sor, and ES-Lma, the ensemble averages of the prior simulated GPP were only approximately half of the observations. After the assimilation of COS, GPP simulations exhibited a significant increase, aligning well with observations at DK-Sor and ES-Lma. Conversely, substantial overestimation in prior GPP simulations was effectively corrected through the assimilation of COS at US-Wrc, resulting in a remarkable enhanced modeling performance in both RMSE and range width. For FI-Hyy and US-Ha1, minimal differences were observed between the ensemble mean of prior and posterior simulations, as the prior simulated GPP had already consistently fit the observations. Nevertheless, our results highlight notable enhancements in the predictive uncertainty of GPP through COS assimilation. In **Fig. 3d**, it is evident that, likely due to the absence of in situ meteorological data at IT-Soy, GPP trends are not well represented, although the ensemble averages of the GPP simulations are very close to the observations in magnitude. However, with a reduction of range width as high as 60.39 %, our finding suggest that the assimilation of COS can significantly reduce the predictive uncertainty of GPP, despite the presence of substantial meteorological data uncertainty.

Table 4. Comparison of model performance indices for the prior and posterior GPP simulations. The $RMSE_{mean}$ of the prior and posterior simulations are the mean values of the RMSEs of 20,000 prior GPP simulations and 100 behavioral GPP simulations with GPP observations, respectively. The range widths of the prior and posterior GPP simulations are defined as the mean values of the difference between the 95th and 5th percentiles of the prior and posterior simulations, respectively.

Site name	$RMSE_{mean}$ (umol m^{-2} s^{-1})			Range width (umol m^{-2} s^{-1})		
	Prior	Posterior	Reduction (%)	Prior	Posterior	Reduction (%)
AT-Neu	11.48	9.30	18.99	17.52	11.84	32.40
DK-Sor	16.51	7.51	54.52	18.04	12.14	32.71
ES-Lma	6.70	5.27	21.43	10.55	7.09	32.75
FI-Hyy	5.49	3.60	34.34	27.50	9.65	64.92
IT-Soy	10.93	7.59	30.60	20.54	8.14	60.39
US-Ha1	6.74	5.30	21.43	31.61	10.71	66.11
US-Wrc	19.08	6.37	66.64	41.89	11.09	73.53

https://doi.org/10.5194/egusphere-2023-3032
Preprint. Discussion started: 22 January 2024

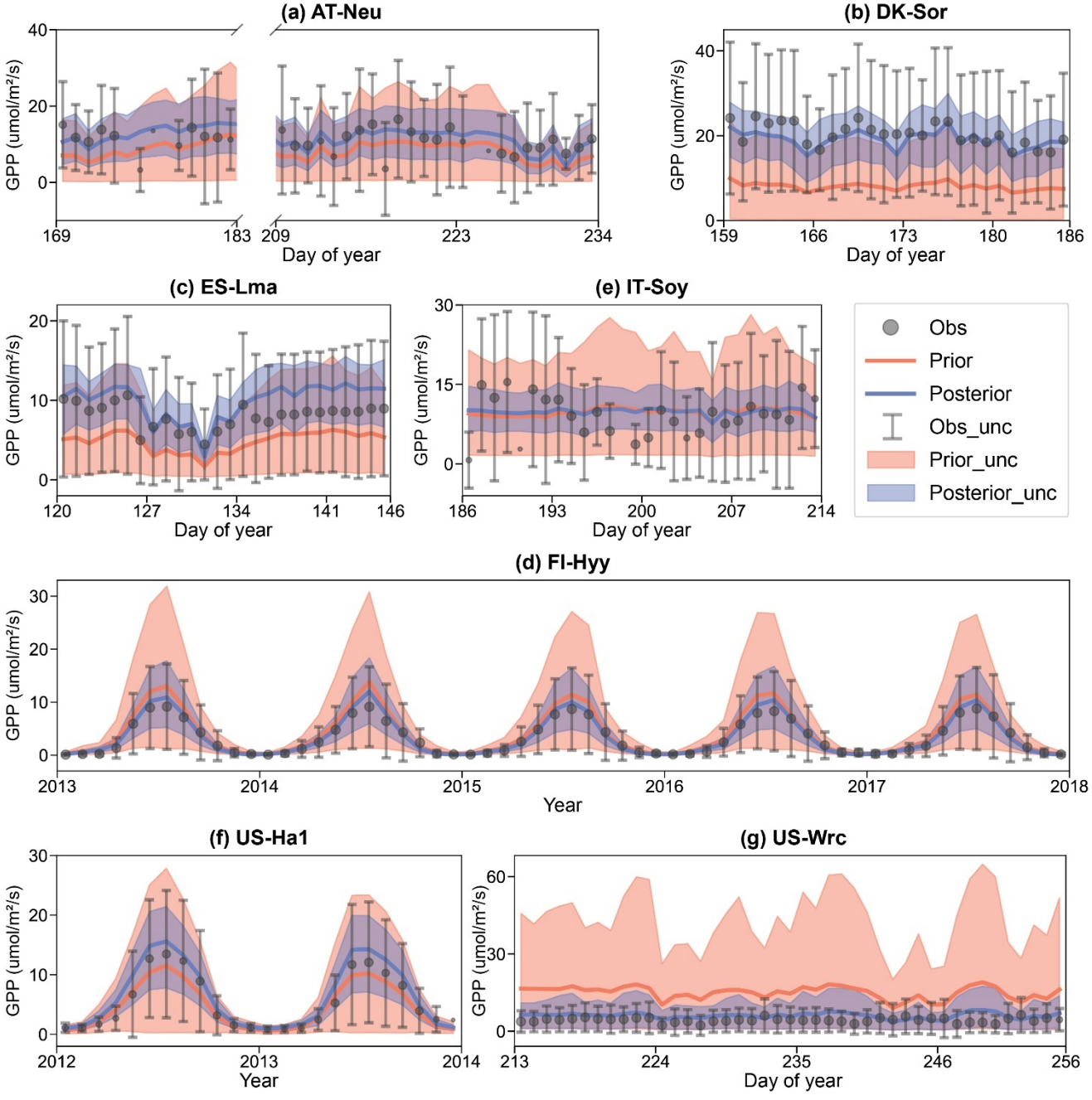

Figure 4. Comparison of prior and posterior simulated GPP. The ensemble means of the prior (red) and posterior (green) simulations are plotted around the uncertainty bounds (5th and 95th quantile). The mean observed GPP and its uncertainty (± 1 standard deviation) are represented by blue dots with error bars. The means and uncertainties of these observations and simulations are calculated and plotted on a daily or monthly scale. Particularly, error bars are not plotted when more than 3/4 of the observations are missing.

https://doi.org/10.5194/egusphere-2023-3032
Preprint. Discussion started: 22 January 2024

4 Discussion

4.1 Parameter sensitivity

As mentioned before, here we utilize the conductance analog model proposed by Berry et al. (2013) to simulate COS plant uptake. Thus, it is not surprised that both the stomatal conductance related parameter b_{H_2O} and m_{H_2O} would impact the modeling of COS flux. Specifically, considering the stress of soil moisture on stomatal conductance, the stomatal conductance was calculated by a modified version (Woodward et al., 1995; Ju et al., 2010) of the Ball-Berry model (Ball et al., 1987) based on the close relationship of stomatal conductance and photosynthesis rate. Consequently, both the soil hydrology related parameters and the photosynthesis related parameters can ultimately play roles in the simulation of COS plant uptake by influence the modeling of stomatal conductance.

It has been recognized that the photosynthetic capacity simulated by terrestrial ecosystem models is highly sensitive to V_{cmax}, J_{max}, and light conditions (Zaehle et al., 2005; Bonan et al., 2011; Rogers, 2014; Sargsyan et al., 2014; Koffi et al., 2015; Rogers et al., 2017; Xing et al., 2023). Our study corroborates these findings, highlighting the pronounced sensitivity of simulated GPP to V_{cmax25}, followed by VJ_{slope} and f_{leaf}. Specifically, our results reveal that GPP simulations exhibit lower sensitivity to f_{leaf} at ES-Lma, where ample light is available but vegetation is sparse (El-Madany et al., 2018; Spielmann et al., 2019), whereas at DK-Sor and US-Ha1, GPP simulations are more sensitive to VJ_{slope}, attributed to the dense vegetation cover (Wehr et al., 2017; Braendholt et al., 2018; Spielmann et al., 2019). Furthermore, our results reveal that the COS simulations are not notably sensitive to f_{leaf} and VJ_{slope} while V_{cmax25} plays a crucial role in the modeling of COS. It is because V_{cmax25} not only affects the estimation of stomatal conductance through photosynthesis, but also is used to characterize the apparent conductance for COS uptake from the intercellular airspaces, as both mesophyll conductance and carbonic anhydrase activity tend to scale with V_{cmax} (Badger and Price, 1994; Evans et al., 1994; Berry et al., 2013). Yet, as the hydrolysis reaction of COS by carbonic anhydrase is not dependent on light, VJ_{slope} and f_{leaf} do not play any roles in the modeling of apparent conductance and thus have little effect on the simulation of COS.

As the COS plant uptake and photosynthesis are tightly coupled through stomata, one would naturally expect similar sensitivity in simulated COS and GPP to stomatal conductance related parameters m_{H_2O} and b_{H_2O}. However, the relationship between COS and stomatal conductance significantly differs from that of GPP and stomatal conductance within the model (e.g., Eq. A18 and the Ball-Berry model). Consequently, a notable difference in sensitivity between simulated GPP and COS to m_{H_2O} and b_{H_2O} was identified in this study. Specifically, m_{H_2O} exhibited more pronounced effects on photosynthesis, while b_{H_2O} played a crucial role in the simulation of COS.

Given that a significant portion of nitrogen is invested in photosynthetic machinery (Mu and Chen, 2021), there exists a close association between leaf nitrogen content and leaf photosynthetic capacity (Sage and Pearcy, 1987). Additionally, the well-established relationship between leaf nitrogen content and carboxylation capacity (Kattge et al., 2009; Lu et al., 2022) further emphasizes this connection. In specific, carboxylation capacity in leaf scale is assumed to be linearly related to leaf nitrogen

https://doi.org/10.5194/egusphere-2023-3032
Preprint. Discussion started: 22 January 2024

content in the BEPS model (Medlyn et al., 1999; Chen et al., 2012). Consequently, both V_{cmax25} and N_{leaf} play crucial roles in influencing carboxylation capacity, thus having a substantial impact on the simulation of COS.

The soil hydrology related parameters can also affect the simulation of COS plant flux as we take the stress effect of soil moisture on both stomatal conductance and mesophyll conductance into account (Ju et al., 2010; Knauer et al., 2020). These parameters also affect the modeling of COS soil exchange since soil moisture is a significant factor in COS soil biotic flux (Whelan et al., 2016). However, given the comparatively smaller magnitude of soil COS exchange compared to plant uptake (Whelan et al., 2018) and the minimal impact of soil moisture stress on photosynthetic capacity (Ma et al., 2022), these soil hydrology relevant parameters do not significantly influence the modeling of COS.

4.2 Parameter interactions

For all seven sites, Pearson correlation coefficients and confident levels between the selected parameters were calculated, as depicted in **Fig. 5** and **Fig. C1**. Generally, each site exhibits approximately 4 to 10 parameter combinations with significant correlations ($p < 0.05$). A total of 14 parameter combinations demonstrate significantly correlated at more than one site, while 10 parameter combinations exhibit significant correlations at only one site. Specifically, with a mean correlation coefficient of -0.48 ± 0.21 (negative value representing a negative correlation), the correlations between V_{cmax25} and N_{leaf} are very significant ($p < 0.01$) at almost all sites (6/7), indicating a robust interaction between them. In addition to V_{cmax25} and N_{leaf}, four parameter combinations show highly significant correlations ($p < 0.01$) at a minimum of two sites, they are b_{H_2O} and f_{leaf}, b_{H_2O} and m_{H_2O}, m_{H_2O} and V_{cmax25}, m_{H_2O} and VJ_{slope}, N_{leaf} and VJ_{slope}, respectively. Such results indicate the strong interactions among plant growth-related parameters, even if some of them do not significantly impact the modeling of COS. In contrast, with a maximum absolute value of 0.26 for the correlation coefficient, soil hydrology related parameters do not exhibit highly significantly correlations with any parameters (except at DK-Sor), indicating their weak equivalence (Wu et al., 2019).

https://doi.org/10.5194/egusphere-2023-3032
Preprint. Discussion started: 22 January 2024

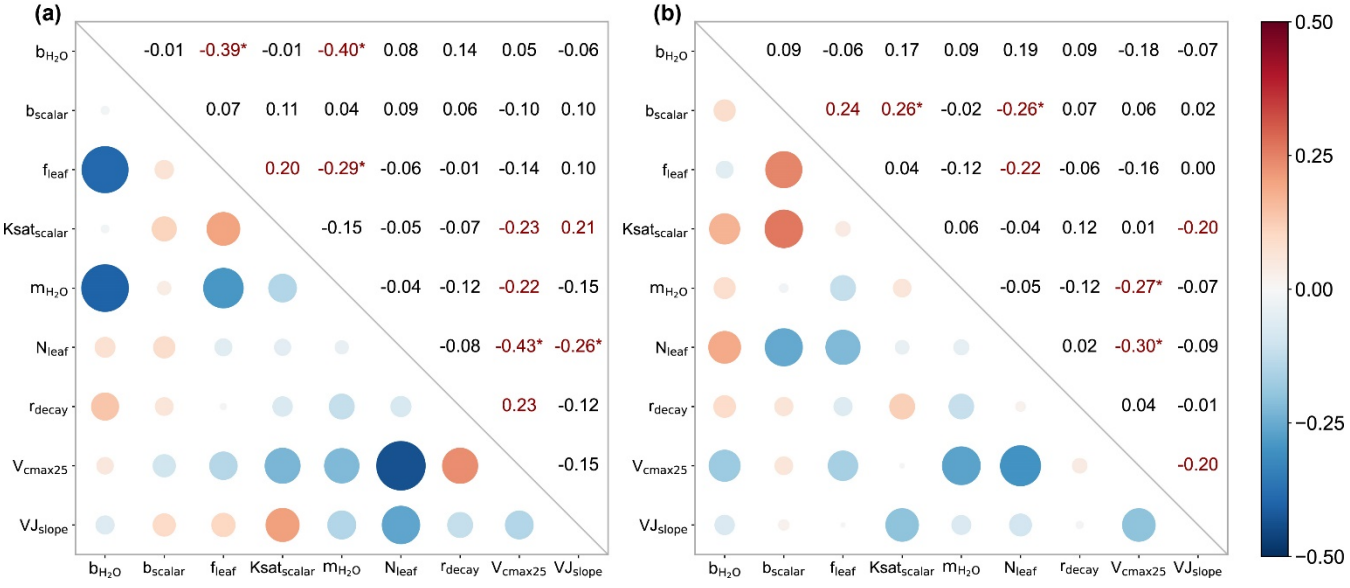

Figure 5. Parameter correlation matrix plots with significance levels between the parameters of the behavioral parameter sets at AT-Neu (a) and DK-Sor (b). Correlation coefficients are shown in red font when the confidence level is greater than 95 % ($p < 0.05$), with a superscript "*" indicating the confidence level greater than 99 % ($p < 0.01$).

We also observed substantial variations in parameter interactions across different sites. For instance, at IT-Soy, b_{H_2O} and f_{leaf} exhibited a highly significant negative correlation with a correlation coefficient as high as -0.49. However, these two parameters seemed irrelevant at US-Wrc with a correlation coefficient of only -0.02. As for soil hydrology related parameters, none of them showed significant correlations with any parameter at IT-Soy, US-Ha1 and US-Wrc, yet there were four parameter combinations related to them significantly correlated at DK-Sor (**Fig. 5b**). Furthermore, while V_{cmax25} is highly correlated with N_{leaf} at all sites, the correlation coefficients varied considerably, ranging from -0.24 to -0.93.

We also observed interactions not only between two parameters but also among several parameters (e.g. b_{H_2O} - f_{leaf} - m_{H_2O} in **Fig. 5a**). To provide deeper insights into these interactions and highlight significantly correlated parameter combinations, we generated **Fig. 6**. This figure not only elucidates the distribution of behavioral parameter sets but also captures the intricate interactions among corresponding parameters. Specifically, the parameter combinations depicted in **Fig. 6** are particularly representative as they originate from diverse sites and include nearly all highly significant correlated combinations. Overall, since all six plant growth related parameters used in this study are positively correlated with the simulation of COS, they consistently constrain each other, demonstrating a negative correlation, as shown in **Fig. 6a**, **Fig. 6c**, and **Fig. 6d**. However, due to the nonlinearity of the model, there is not a simple linear relationship between these parameters. For example, at ES-Lma, where the COS observations significantly surpass the ensemble mean of prior simulations, V_{cmax25} and VJ_{slope} are not linearly correlated with each other, but are both well confined to the region around their upper limits (**Fig. 6b**).

https://doi.org/10.5194/egusphere-2023-3032
Preprint. Discussion started: 22 January 2024

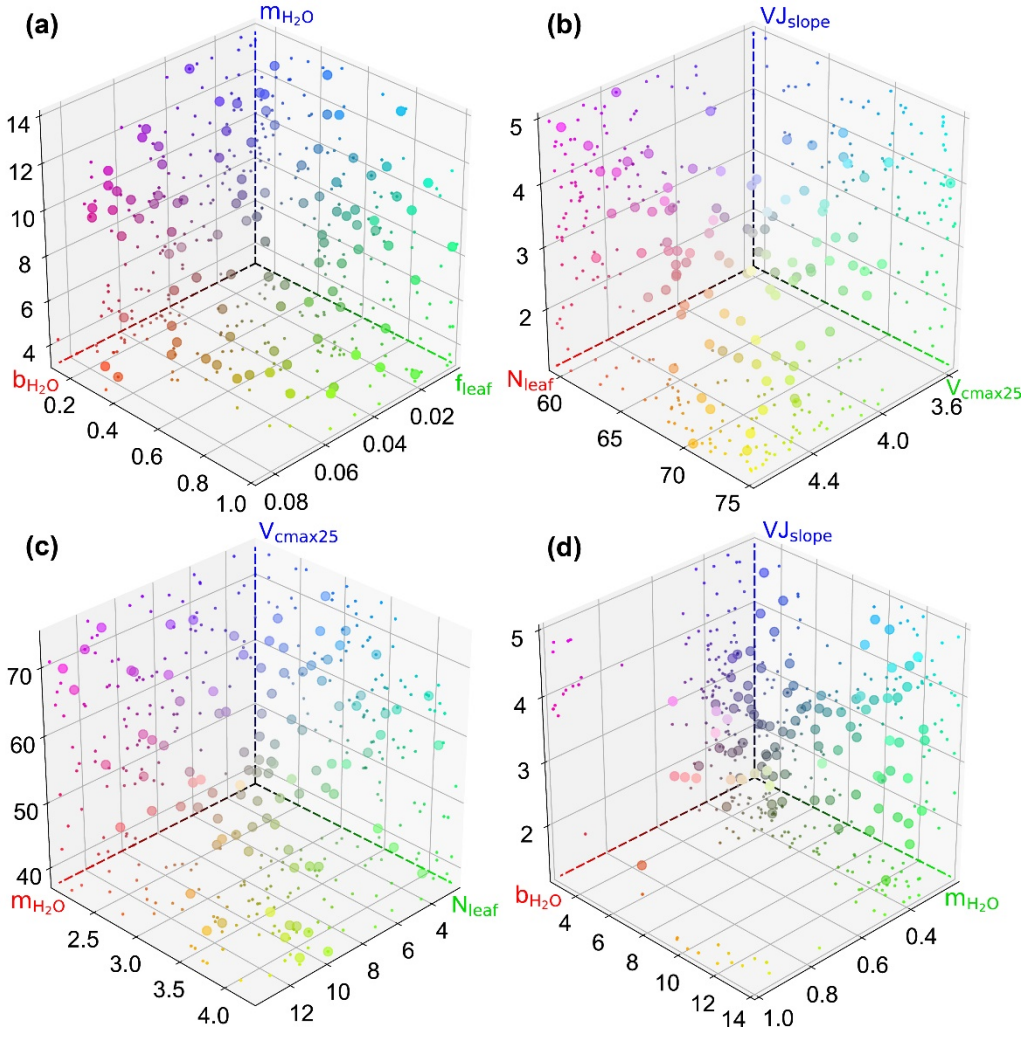

Figure 6. Scatter plots showing the behavioral parameter sets in 3D parameter space at AT-Neu (a), ES-Lma (b) and US-Ha1 (c) and US-Wrc. The scatter colors represent the magnitude of the corresponding parameters using RGB values. The projection of the scatter is illustrated with smaller markers.

4.3 Parameter identifiability

As the parameter identifiability is quantified based on the range of the behavioral parameter, its results were presented in **Fig. 2** along with the plots of the cumulative likelihood distributions of the behavioral parameters. These results underscore the remarkable ability of COS assimilation to identify b_{H_2O}, with a mean PI of b_{H_2O} as high as 0.76 ± 0.25. Identified as the most sensitive parameters for COS modeling, V_{cmax25} and N_{leaf} also exhibit remarkable identifiability, with mean PIs of 0.39 ± 0.25 and 0.42 ± 0.19 respectively. The other three plant growth-related parameters (m_{H_2O}, VJ_{slope} and f_{leaf}) demonstrate varying levels of identifiability, with PIs ranging from 0.06 to 0.42, 0.03 to 0.30, and 0 to 0.09, respectively. While these

https://doi.org/10.5194/egusphere-2023-3032
Preprint. Discussion started: 22 January 2024

parameters are well identified at some sites, they prove almost unidentifiable at others. Notably, VJ_{slope} achieves optimal identification at DK-Sor, where its PI is approximately eight times that of the other sites.

The identifiability of a parameter with input data closely correlates with the sensitivity of the input data to the parameter, although it can be influenced by model over-parameterization and parameter interactions (Gan et al., 2014). For instance, our results demonstrate the orders of sensitivity and identifiability for V_{cmax25} and N_{leaf} are almost consistent at the same site (**Fig. 2**). Given the high sensitivity of COS modeling to V_{cmax25}, N_{leaf} and b_{H_2O}, it is unsurprising that these parameters can be effectively identified by the assimilation of COS. However, our findings indicate that the sensitivity of V_{cmax25}, N_{leaf} is much greater than that of b_{H_2O}, yet the latter is much more identifiable. This outcome can be attributed to the highly significant correlation between V_{cmax25} and N_{leaf}, as parameter interaction is a primary contributor to parameter unidentifiability (Gan et al., 2014).

In Sect. 3.1, it was demonstrated that the modeling of COS exhibits low sensitivity to f_{leaf}, m_{H_2O} and VJ_{slope}. Consequently, it is reasonable that the assimilation of COS may not effectively identify f_{leaf}, m_{H_2O} and VJ_{slope} at certain sites (**Fig. 2**). However, due to their significant correlations with other plant growth-related parameters, effective identification is possible in specific cases. Notably, combinations such as f_{leaf}-N_{leaf}, m_{H_2O}-V_{cmax25} and V_{cmax25}-VJ_{slope} are significantly correlated (**Fig. 5b**), and both N_{leaf} and V_{cmax25} were effectively identified at DK-Sor. As a result, f_{leaf}, m_{H_2O} and VJ_{slope} also attain highly identifiability at this site.

It has been previously demonstrated that soil hydrology-related parameters exert a minimal impact on COS simulations and cannot be effectively constrained through COS assimilation. Consequently, these parameters exhibit low identifiability, although significant combinations of correlations associated with soil hydrology-related parameters were observed at certain sites (e.g., DK-Sor).

4.4 Relationship between COS and GPP simulation performance

In this study, we identified the top 100 parameter sets, whose corresponding simulations displayed the smallest RMSE concerning COS observations, as the behavioral parameter sets. Subsequently, these sets were employed to derive the posterior simulated COS and GPP, and to estimate prediction uncertainty. Therefore, it is necessary to investigate how COS simulations and GPP simulations respond to RMSE and to understand the relationship between the model performance of COS and that of GPP.

https://doi.org/10.5194/egusphere-2023-3032
Preprint. Discussion started: 22 January 2024

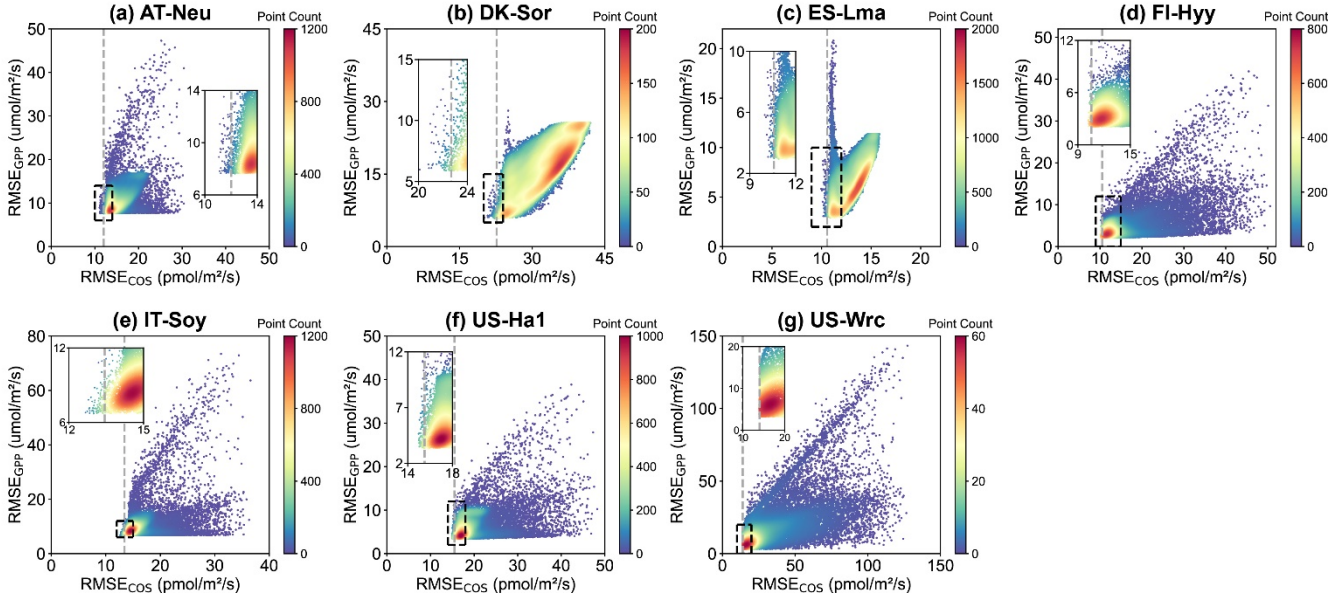

Figure 7. Comparison of RMSE for COS (RMSE$_{COS}$) and GPP (RMSE$_{GPP}$) in the Monte Carlo simulations. Each data point represents a parameter set, with color indicating data density. The gray dashed line represents the RMSE threshold for COS simulation, calculated as the mean of the 100th and 101st smallest values of the RMSE.

In **Fig.7**, scatter plots of RMSEs for COS and GPP are presented. It can be observed that at most sites, where the scatters are most densely distributed, there tend to be relatively small RMSEs for both COS and GPP. These results indicate that the current model is generally capable to simulate COS and GPP well at the same time. However, given the uncertainties of model parameters, structure and driving data etc., instances like at ES-Lma arise where numerous parameter combinations simultaneously exhibit a small RMSE for COS, but their RMSE values for GPP show a significant range of variation. Moreover, due to the noticeable differences in the mechanisms of COS and GPP, such as that the photosynthetic rate in the Farquhar photosynthesis model (Farquhar et al., 1980) is limited either by the RuBP (ribulose-1,5-bisphosphate) carboxylation or by the RuBP regeneration (Hikosaka et al., 2006), while the current modeling of COS is insensitive to the parameters related to RuBP regeneration (e.g. VJ_{slope} and f_{leaf}), numerous parameter sets of these sites perform well for either COS or GPP but exhibit significant discrepancies with the observations of the other. More specifically, our results suggest that these behavioral parameter sets, which demonstrate good performance in COS simulation, also generally perform well in modeling GPP. However, the parameter sets with relatively good GPP simulation results exhibit significant variability in the performance of COS modeling.

5 Conclusions

In this study, carbonyl sulfide flux data were utilized to calibrate the ecosystem model parameters and to optimize GPP simulations among various ecosystems within the Monte Carlo-based methodology base on the coupling of COS modeling

https://doi.org/10.5194/egusphere-2023-3032
Preprint. Discussion started: 22 January 2024

and the BEPS model. Global parameter sensitivity analysis was conducted to identify the sensitive parameters for COS and GPP modeling, the identifiability and interaction of model parameters were investigated by the behavioral parameter sets. The major findings are as follows:

(1) Similar to GPP, we found the modeling of COS is sensitive to parameters V_{cmax25}, N_{leaf} and b_{H_2o}, while insensitive to soil hydrology related parameters. Unlike GPP, COS is also insensitive to m_{H_2o} and the light-reaction related parameters VJ_{slope} and f_{leaf}.

(2) The assimilation of COS within the Monte Carlo-based approach effectively improved model performance of GPP and significantly reduced the model predictive uncertainty, with a mean RMSE reduction of 35.42 % ± 17.01 % and a mean range width reduction as high as 51.83% ± 17.02 %.

(3) Complex and significant two-parameter or multi-parameter interactions exists between the model parameters. In particularly, V_{cmax25} and N_{leaf} are significantly correlated ($p < 0.05$) at all sites.

(4) Generally, b_{H_2o}, V_{cmax25} and N_{leaf} can be well identified through the assimilation of COS, especially b_{H_2o}, whereas the soil hydrology related parameters cannot be identified effectively. m_{H_2o}, VJ_{slope} and f_{leaf} can also be effectively identified due to strong parameter interactions.

Appendix A:

A1 BEPS photosynthesis and stomatal conductance modeling approach

In the BEPS model, the net photosynthesis rate (A) is calculated using the Farquhar model (Farquhar et al., 1980; Chen et al., 1999):

$$\mathrm{A} = \min(A_i, A_j) - R_d \quad \text{(A1)}$$

$$A_c = V_{cmax}\frac{C_i - \Gamma_i^*}{C_i + K_c\left(1 + \frac{O_i}{K_o}\right)} \quad \text{(A2)}$$

$$A_j = J\frac{C_i - \Gamma_i^*}{4(C_i - 2\Gamma_i^*)} \quad \text{(A3)}$$

where A_i and A_j are Rubisco-limited and RuBP-limited gross photosynthetic rates (μmol $m^{-2}s^{-1}$), respectively. R_d is leaf dark respiration (μmol $m^{-2}s^{-1}$). V_{cmax} is the maximum carboxylation rate of Rubisco (μmol $m^{-2}s^{-1}$); J is the electron transport rate (μmol $m^{-2}s^{-1}$); Ci and Oi are the intercellular carbon dioxide (CO_2) and oxygen (O_2) concentrations (mol mol^{-1}), respectively; Kc and Ko are Michaelis–Menten constants for CO_2 and O_2 (mol mol^{-1}), respectively.

The electron transport rate, J, is dependent on incident photosynthetic photon flux density (PPFD, μmol $m^{-2}s^{-1}$) as:

$$\mathrm{J} = \frac{J_{max}\, I}{I + 2.1J_{max}} \quad \text{(A4)}$$

where J_{max} is the maximum electron transport rate (μmol $m^{-2}s^{-1}$), I is the incident PPFD calculated from the incident shortwave radiation R_{SW} (W m^{-2}):

https://doi.org/10.5194/egusphere-2023-3032
Preprint. Discussion started: 22 January 2024

$$I = \beta\, R_{SW}\, f_{leaf} \tag{A5}$$

where $\beta = 4.55$ is the energy – quanta conversion factor (μmol J^{-1}), f_{leaf} is the ratio of photosynthesis active radiation to the shortwave radiation (unitless).

The maximum carboxylation rate of Rubisco V_{cmax} was calculated according the Arrhenius temperature function and the maximum carboxylation rate of Rubisco at 25 ℃ (V_{cmax25}). V_{cmax} is generally proportional to leaf nitrogen content. Considering both the fractions of sunlit and shaded leaf areas to the total leaf area and the leaf nitrogen content vary with the depth into the canopy, the V_{cmax} values of sunlit ($V_{cmax,sun}$) and shaded ($V_{cmax,sh}$) leaves can be obtained through vertical integrations with respect to leaf area index (L) (Chen et al., 2012):

$$V_{cmax,sun} = V_{cmax}\chi_n N_{leaf}\frac{k\left[1-e^{(k_n+k)L}\right]}{(k_n+k)(1-e^{-kL})} \tag{A6}$$

$$V_{cmax,sh} = V_{cmax}\chi_n N_{leaf}\frac{\frac{1}{k_n}\left[1-e^{-K_nL}\right]-\frac{1}{k_n+k}\left[1-e^{(k_n+k)L}\right]}{L-\frac{1}{k}(1-e^{-kL})} \tag{A7}$$

where χ_n ($m^2\ g^{-1}$) is the relative change of V_{cmax} to leaf nitrogen content; N_{leaf} ($g\ m^{-2}$) is the leaf nitrogen content at the top of the canopy; k_n (unitless) is the leaf nitrogen content decay rate with increasing depth into the canopy, taken as 0.3; k is calculated as:

$$k = G(\theta)\Omega\, cos(\theta) \tag{A8}$$

where G(θ) is the projection coefficient, taken as 0.5, Ω is the clumping index, and θ is the is the solar zenith angle.

After V_{cmax} values for the representative sunlit and shaded leaves are obtained, the maximum electronic transport rate for the sunlit and shaded leaves are obtained from Medlyn et al. (1999):

$$J_{max} = VJ_{slope}\, V_{cmax} - 14.2 \tag{A9}$$

where VJ_{slope} (unitless) is the slope of the relationship of V_{cmax} and J_{max}.

The leaf stomatal conductance to water vapor (g_{sw} in) is estimated using a modified version of Ball-Berry (BB) empirical model (Ball et al., 1987) following Woodward et al. (1995):

$$g_{sw} = b_{H_2O} + \frac{m_{H_2O}\, A\ R_h\, f_w}{C_a} \tag{A10}$$

where b_{H_2O} is intercept of the Ball-Berry model, representing the minimum g_{sw} (mol $m^{-2}s^{-1}$), m_{H_2O} is the empirical slope parameter in the BB model (unitless), R_h is the relative humidity at the leaf surface (unitless), f_w is a soil moisture stress factor describing the sensitivity of g_{sw} to soil water availability (Ju et al., 2006), C_a is the atmospheric CO_2 concentration (μmol mol^{-1}).

Soil water availability factor $f_{w,i}$ in each layer *i* is calculated as:

$$f_{w,i} = \frac{1.0}{f_i(\psi_i)f_i(T_{s,i})} \tag{A11}$$

https://doi.org/10.5194/egusphere-2023-3032
Preprint. Discussion started: 22 January 2024

where $f_i(\psi_i)$ is a function of matrix suction ψ_i (m) (Zierl, 2001), $f_i(T_{s,i})$ is a function describing the effect of soil temperature ($T_{s,i}$ in ℃) on soil water uptake (Bonan, 1991).

To consider the variable soil water potential at different depths, the scheme of Ju et al. (2006) was employed to calculate the weight of each layer (w_i) to f_w:

$$w_i = \frac{R_i f_{w,i}}{\sum_{i=1}^{n} R_i f_{w,i}} \tag{A12}$$

where n is the number of soil layer (five were used in this study) of the BEPS model, R_i is the root fraction in layer i, calculated as:

$$R_i = \begin{cases} 1 - {r_{decay}}^{100cd_i} & i = 1 \\ {r_{decay}}^{100cd_{i-1}} - {r_{decay}}^{100cd_i} & 1 < i < n \\ {r_{decay}}^{100cd_{i-1}} & i = n \end{cases} \tag{A13}$$

where cd_i is the cumulative thickness (m) of layer i. In this study, each soil layer depth (from top to bottom) of the BEPS model is 0.05 m, 0.10 m, 0.20 m, 0.40 m and 1.25 m, respectively.

The overall soil water availability f_w is then calculated as:

$$f_w = \sum_{i=1}^{n} f_{w,i} w_i \tag{A14}$$

The hydraulic conductivity of each soil layer K_i (m s^{-1}) is expressed as:

$$K_i = Ksat_i \left(\frac{swc_i}{\theta_{s,i}}\right)^{2b_i+3} \tag{A15}$$

where $Ksat_i$ is the saturated hydrological conductivity of soil layer i (m s^{-1}); SWC_i is the volumetric liquid soil water content of soil layer i (m s^{-1}); $\theta_{s,i}$ is the porosity of soil layer i (unitless); b_i is the Campbell parameter for soil layer i, determining the change rate of hydraulic conductivity with SWC (unitless). In this study, $Ksat_i$ and b_i are expressed as:

$$Ksat_i = Ksat_{scalar} Ksat_{df,i} \tag{A16}$$

$$b_i = b_{scalar} b_{df,i} \tag{A17}$$

where $Ksat_{df,i}$ and $b_{df,i}$ are the default values of $Ksat_i$ and b_i respectively.

A2 BEPS leaf COS modeling approach

The leaf-level COS uptake rate $F_{cos,leaf}$ is determined by the formula:

$$F_{cos,leaf} = cos_a \left(\frac{1.94}{g_{sw}} + \frac{1.56}{g_{bw}} + \frac{1}{g_{cos}}\right)^{-1} \tag{A18}$$

where cos_a represents the COS mole fraction in the bulk air. g_{sw} and g_{bw} are the stomatal conductance and leaf laminar boundary layer conductance to H_2O vapor. g_{cos} indicates the apparent conductance for COS uptake from the intercellular

https://doi.org/10.5194/egusphere-2023-3032
Preprint. Discussion started: 22 January 2024

airspaces, which combined the mesophyll conductance and the biochemical reaction rate of COS and carbonic anhydrase. It can be calculated as:

$$g_{cos} = 1.4 * 10^3 * (1.0 + 5.33 * F_{C4}) * 10^{-6} * \left(1 - e^{(-0.45*LAI)}\right) f_{sw} V_{cmax} \quad \text{(A19)}$$

where F_{C4} denotes the C4 plant flag, taking the value of 1 for C4 plants and 0 otherwise. f_{sw} is a parameter describing soil water stress.

The total soil COS flux $F_{cos,soil}$ is the sum of abiotic COS flux $F_{cos,abiotic}$ and biotic COS flux $F_{cos,biotic}$.

$$F_{cos,soil} = F_{cos,abiotic} + F_{cos,biotic} \quad \text{(A20)}$$

Here, we take the approach developed in Whelan et al. (2016) for the modeling of $F_{cos,soil}$. In this approach, $F_{cos,abiotic}$ is described as an exponential function of the temperature of soil T_{soil} (℃).

$$F_{cos,abiotic} = \alpha e^{\beta T_{soil}} \quad \text{(A21)}$$

where α and β were parameters determined using the least-squares fitting approach. We assigned the values of α and β to BEPS according to the parameterizations scheme of Abadie et al. (2022).

$F_{cos,biotic}$ is described as the product of a power function and an exponential function.

$$F_{cos,biotic} = F_{opt} \left(\frac{SWC}{SWC_{opt}}\right) e^{-a\left(\frac{SWC}{SWC_{opt}}-1\right)} \quad \text{(A22)}$$

$$a = ln\left(\frac{F_{opt}}{F_{SWC_g}}\right)\left(ln\left(\frac{SWC_{opt}}{SWC_g}\right) + \left(\frac{SWC_g}{SWC_{opt}} - 1\right)\right)^{-1} \quad \text{(A23)}$$

here a is the curve shape constant. The maximum biotic COS uptake F_{opt} and the biotic COS uptake F_{SWC_g} are the COS fluxes (pmol m^{-2} s^{-1}) at optimum soil water content SWC_{opt} and a secondary soil water content SWC_g, and $SWC_g > SWC_{opt}$. A more detailed description of the modeling of $F_{cos,biotic}$ and the parameterization scheme adopted in this study can be found in Whelan et al. (2022).

Appendix B: Additional table

Table B1. Descriptions of the 9 parameters were selected to be calibrated. The default values and prior ranges (in parentheses) of these parameters are given for each plant function type (PFT) or for each soil texture or globally according to the parameter dependent.

Parameter	Description	Dependent	Default value and prior range				
			ENF/ Loamy sand	DBF/Loam	Grass/ Silty loam	Crop/Sandy clay loam	Silty clay
b_{H_2O}	The intercept of the Ball-Berry model (mol $m^{-2}s^{-1}$)	PFT	0.0175 (0.004375-1)	0.0175 (0.004375-1)	0.0175 (0.004375-1)	0.0175 (0.004375-1)	
b_{scalar}	The scaling factor of Campbell parameter b	Texture	1 (0.25-0.75)	1 (0.25-0.75)	1 (0.25-0.75)	1 (0.25-0.75)	1 (0.25-0.75)
f_{leaf}	Ratio of photosynthetically active radiation to shortwave radiation	Global	0.5 (0.125-1)				

https://doi.org/10.5194/egusphere-2023-3032
Preprint. Discussion started: 22 January 2024

$Ksat_{scalar}$	The scaling factor of saturated hydraulic conductivity Ksat	Texture	1 (0.25-0.75)	1 (0.25-0.75)	1 (0.25-0.75)	1 (0.25-0.75)	1 (0.25-0.75)
m_{H_2O}	The slope of the Ball-Berry model	PFT	8 (2-14)	8 (2-14)	8 (2-14)	8 (2-14)	
N_{leaf}	Leaf nitrogen content ($m^2\ g^{-1}$)	PFT	4.45 (1-7.7875)	2.45 (1-4.2875)	2.695 (1-4.71625)	2.375 (1-4.15625)	
r_{decay}	Decay rate of root distribution	PFT	0.95 (0.2375-0.99)	0.97 (0.2425-0.99)	0.96 (0.24-0.99)	0.95 (0.2375-0.99)	
V_{cmax25}	Maximum carboxylation rate of Rubisco at 25 °C (μmol $m^{-2}s^{-1}$)	PFT	62.5 (15-75)	57.7 (15-75)	48 (15-75)	84.5 (15-120)	
VJ_{slope}	Slope of the V_{cmax} and J_{max} (maximum electron transport rate) relationship	PFT	2.39 (1-5)	2.39 (1-5)	2.39 (1-5)	2.39 (1-5)	

Appendix C: Additional figure

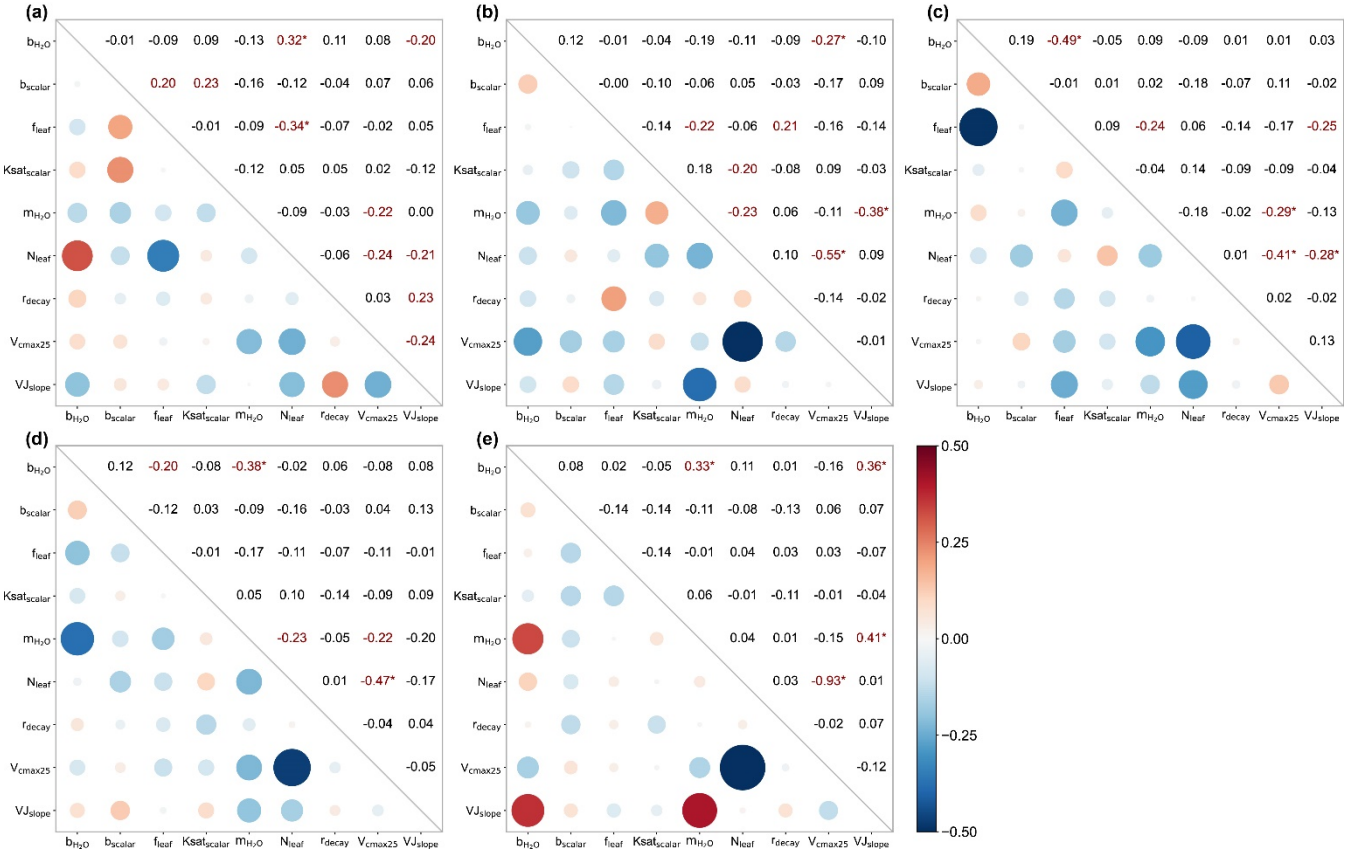

595 **Figure C1.** Parameter correlation matrix plots with significance levels between the parameters of the behavioral parameter sets at ES-Lma (a), FI-Hyy (b), IT-Soy (c), US-Ha1 (d) and US-Wrc (e). Correlation coefficients are shown in red font when the correlation confidence level is greater than 95 % ($p < 0.05$), with a superscript "*" indicating a confidence level greater than 99 % ($p < 0.01$).

https://doi.org/10.5194/egusphere-2023-3032
Preprint. Discussion started: 22 January 2024

Data availability. Measured eddy covariance carbonyl sulfide fluxes data can be found at https://zenodo.org/record/3406990 for AT-Neu, DK-Sor, ES-Lma and IT-Soy, https://zenodo.org/record/6940750 for FI-Hyy, and from the Harvard Forest Data Archive under record HF214 (https://portal.edirepository.org/nis/mapbrowse?packageid=knb-lter-hfr.214.4) for US-Ha1.The raw COS concentration data of US-Wrc can be obtained at https://zenodo.org/record/1422820. The meteorological data can be obtained from the FLUXNET database (https://fluxnet.org/) for AT-Neu, DK-Sor, ES-LMa, FI-Hyy; from the AmeriFlux database (https://ameriflux.lbl.gov/) for US-Ha1 (except shortwave radiation data) and US-Wrc; from the ERA5 dataset (https://cds.climate.copernicus.eu/cdsapp#!/dataset/reanalysis-era5-single-levels?tab=overview) for AT-Neu, IT-Soy and US-Ha1. The GPP data can be obtained from the FLUXNET database for DK-Sor, ES-LMa, FI-Hyy; from the AmeriFlux database for US-Ha1 and US-Wrc; and from https://zenodo.org/record/6940750 for AT-Neu and IT-Soy. The GLOBMAP LAI is available at https://zenodo.org/record/4700264#.YzvSYnZBxD8%2F ,the GLASS LAI is available at ftp://ftp.glcf.umd.edu/, the MODIS LAI product is available at https://lpdaac.usgs.gov/products/mod15a2hv006/.

Author contributions.

MW designed the experiments and developed the model, XX improved the model and performed the Monte Carlo simulations, HZ wrote the original manuscript and made the analysis. All the authors contributed to the writing of the manuscript.

Competing interests. The authors declare that they have no conflict of interest.

Acknowledgements. This study was supported by the National Natural Science Foundation of China (42371486, 42111530184), the Research Funds for the Frontiers Science Center for Critical Earth Material Cycling, Nanjing University (Grant No: 090414380031, 020914380115).

Reference

Abadie, C., Maignan, F., Remaud, M., Kohonen, K. M., Sun, W., Kooijmans, L., Vesala, T., Seibt, U., Raoult, N., and Bastrikov, V.: Carbon and water fluxes of the boreal evergreen needleleaf forest biome constrained by assimilating ecosystem carbonyl sulfide flux observations, Journal of Geophysical Research: Biogeosciences, e2023JG007407, 2023.

Abadie, C., Maignan, F., Remaud, M., Ogée, J., Campbell, J. E., Whelan, M. E., Kitz, F., Spielmann, F. M., Wohlfahrt, G., and Wehr, R.: Global modelling of soil carbonyl sulfide exchanges, Biogeosciences, 19, 2427-2463, 2022.

Asaf, D., Rotenberg, E., Tatarinov, F., Dicken, U., Montzka, S. A., and Yakir, D.: Ecosystem photosynthesis inferred from measurements of carbonyl sulphide flux, Nature Geoscience, 6, 186-190, 2013.

Badger, M. R. and Price, G. D.: The role of carbonic anhydrase in photosynthesis, Annual review of plant biology, 45, 369-392, 1994.

Ball, J. T., Woodrow, I. E., and Berry, J. A.: A model predicting stomatal conductance and its contribution to the control of photosynthesis under different environmental conditions, Progress in photosynthesis research: volume 4 proceedings of the VIIth international congress on photosynthesis providence, Rhode Island, USA, august 10–15, 1986, 221-224,

Berry, J., Wolf, A., Campbell, J. E., Baker, I., Blake, N., Blake, D., Denning, A. S., Kawa, S. R., Montzka, S. A., and Seibt, U.: A coupled model of the global cycles of carbonyl sulfide and CO2: A possible new window on the carbon cycle, Journal of Geophysical Research: Biogeosciences, 118, 842-852, 2013.

https://doi.org/10.5194/egusphere-2023-3032
Preprint. Discussion started: 22 January 2024

Beven, K. and Binley, A.: The future of distributed models: model calibration and uncertainty prediction, Hydrological processes, 6, 279-298, 1992.
Beven, K. and Binley, A.: GLUE: 20 years on, Hydrological processes, 28, 5897-5918, 2014.
Beven, K. and Freer, J.: Equifinality, data assimilation, and uncertainty estimation in mechanistic modelling of complex environmental systems using the GLUE methodology, Journal of hydrology, 249, 11-29, 2001.
Billesbach, D., Berry, J., Seibt, U., Maseyk, K., Torn, M., Fischer, M., Abu-Naser, M., and Campbell, J.: Growing season eddy covariance measurements of carbonyl sulfide and CO2 fluxes: COS and CO2 relationships in Southern Great Plains winter wheat, Agricultural and Forest Meteorology, 184, 48-55, 2014.
Blankenship, R. E.: Molecular mechanisms of photosynthesis, John Wiley & Sons2021.
Blasone, R.-S., Vrugt, J. A., Madsen, H., Rosbjerg, D., Robinson, B. A., and Zyvoloski, G. A.: Generalized likelihood uncertainty estimation (GLUE) using adaptive Markov Chain Monte Carlo sampling, Advances in Water Resources, 31, 630-648, 2008.
Bonan, G. B.: A biophysical surface energy budget analysis of soil temperature in the boreal forests of interior Alaska, Water Resources Research, 27, 767-781, 1991.
Bonan, G. B., Lawrence, P. J., Oleson, K. W., Levis, S., Jung, M., Reichstein, M., Lawrence, D. M., and Swenson, S. C.: Improving canopy processes in the Community Land Model version 4 (CLM4) using global flux fields empirically inferred from FLUXNET data, Journal of Geophysical Research: Biogeosciences, 116, 2011.
Borgonovo, E.: A new uncertainty importance measure, Reliability Engineering & System Safety, 92, 771-784, 2007.
Braendholt, A., Ibrom, A., Larsen, K. S., and Pilegaard, K.: Partitioning of ecosystem respiration in a beech forest, Agricultural and Forest Meteorology, 252, 88-98, 2018.
Canadell, J., Mooney, H., Baldocchi, D., Berry, J., Ehleringer, J., Field, C., Gower, S. T., Hollinger, D., Hunt, J., and Jackson, R. B.: Commentary: carbon metabolism of the terrestrial biosphere: a multitechnique approach for improved understanding, Ecosystems, 3, 115-130, 2000.
Chen, B., Wang, P., Wang, S., Ju, W., Liu, Z., and Zhang, Y.: Simulating canopy carbonyl sulfide uptake of two forest stands through an improved ecosystem model and parameter optimization using an ensemble Kalman filter, Ecological Modelling, 475, 110212, 2023.
Chen, J., Liu, J., Cihlar, J., and Goulden, M.: Daily canopy photosynthesis model through temporal and spatial scaling for remote sensing applications, Ecological modelling, 124, 99-119, 1999.
Chen, J. M., Ju, W., Ciais, P., Viovy, N., Liu, R., Liu, Y., and Lu, X.: Vegetation structural change since 1981 significantly enhanced the terrestrial carbon sink, Nature communications, 10, 4259, 2019.
Chen, J. M., Mo, G., Pisek, J., Liu, J., Deng, F., Ishizawa, M., and Chan, D.: Effects of foliage clumping on the estimation of global terrestrial gross primary productivity, Global Biogeochemical Cycles, 26, 2012.
Cho, A., Kooijmans, L. M., Kohonen, K.-M., Wehr, R., and Krol, M. C.: Optimizing the carbonic anhydrase temperature response and stomatal conductance of carbonyl sulfide leaf uptake in the Simple Biosphere model (SiB4), Biogeosciences, 20, 2573-2594, 2023.
Commane, R., Meredith, L. K., Baker, I. T., Berry, J. A., Munger, J. W., Montzka, S. A., Templer, P. H., Juice, S. M., Zahniser, M. S., and Wofsy, S. C.: Seasonal fluxes of carbonyl sulfide in a midlatitude forest, Proceedings of the National Academy of Sciences, 112, 14162-14167, 2015.
El-Madany, T. S., Reichstein, M., Perez-Priego, O., Carrara, A., Moreno, G., Martín, M. P., Pacheco-Labrador, J., Wohlfahrt, G., Nieto, H., and Weber, U.: Drivers of spatio-temporal variability of carbon dioxide and energy fluxes in a Mediterranean savanna ecosystem, Agricultural and Forest Meteorology, 262, 258-278, 2018.
Evans, J. R., Caemmerer, S., Setchell, B. A., and Hudson, G. S.: The relationship between CO2 transfer conductance and leaf anatomy in transgenic tobacco with a reduced content of Rubisco, Functional Plant Biology, 21, 475-495, 1994.
Farquhar, G. D., von Caemmerer, S. v., and Berry, J. A.: A biochemical model of photosynthetic CO 2 assimilation in leaves of C 3 species, planta, 149, 78-90, 1980.
Friedlingstein, P., O'sullivan, M., Jones, M. W., Andrew, R. M., Gregor, L., Hauck, J., Le Quéré, C., Luijkx, I. T., Olsen, A., and Peters, G. P.: Global carbon budget 2022, Earth System Science Data Discussions, 2022, 1-159, 2022.
Gan, Y., Duan, Q., Gong, W., Tong, C., Sun, Y., Chu, W., Ye, A., Miao, C., and Di, Z.: A comprehensive evaluation of various sensitivity analysis methods: A case study with a hydrological model, Environmental modelling & software, 51, 269-285, 2014.

https://doi.org/10.5194/egusphere-2023-3032
Preprint. Discussion started: 22 January 2024

Goldan, P. D., Fall, R., Kuster, W. C., and Fehsenfeld, F. C.: Uptake of COS by growing vegetation: A major tropospheric sink, Journal of Geophysical Research: Atmospheres, 93, 14186-14192, 1988.

Gu, L., Baldocchi, D., Verma, S. B., Black, T., Vesala, T., Falge, E. M., and Dowty, P. R.: Advantages of diffuse radiation for terrestrial ecosystem productivity, Journal of Geophysical Research: Atmospheres, 107, ACL 2-1-ACL 2-23, 2002.

He, H., Jansson, P.-E., Svensson, M., Meyer, A., Klemedtsson, L., and Kasimir, Å.: Factors controlling Nitrous Oxide emission from a spruce forest ecosystem on drained organic soil, derived using the CoupModel, Ecological Modelling, 321, 46-63, 2016.

He, Q., Ju, W., Dai, S., He, W., Song, L., Wang, S., Li, X., and Mao, G.: Drought risk of global terrestrial gross primary productivity over the last 40 years detected by a remote sensing-driven process model, Journal of Geophysical Research: Biogeosciences, 126, e2020JG005944, 2021.

Hikosaka, K., Ishikawa, K., Borjigidai, A., Muller, O., and Onoda, Y.: Temperature acclimation of photosynthesis: mechanisms involved in the changes in temperature dependence of photosynthetic rate, Journal of experimental botany, 57, 291-302, 2006.

Hilton, T. W., Whelan, M. E., Zumkehr, A., Kulkarni, S., Berry, J. A., Baker, I. T., Montzka, S. A., Sweeney, C., Miller, B. R., and Elliott Campbell, J.: Peak growing season gross uptake of carbon in North America is largest in the Midwest USA, Nature Climate Change, 7, 450-454, 2017.

Houska, T., Multsch, S., Kraft, P., Frede, H.-G., and Breuer, L.: Monte Carlo-based calibration and uncertainty analysis of a coupled plant growth and hydrological model, Biogeosciences, 11, 2069-2082, 2014.

Hu, L., Montzka, S. A., Kaushik, A., Andrews, A. E., Sweeney, C., Miller, J., Baker, I. T., Denning, S., Campbell, E., and Shiga, Y. P.: COS-derived GPP relationships with temperature and light help explain high-latitude atmospheric CO2 seasonal cycle amplification, Proceedings of the National Academy of Sciences, 118, e2103423118, 2021.

Iwanaga, T., Usher, W., and Herman, J.: Toward SALib 2.0: Advancing the accessibility and interpretability of global sensitivity analyses, Socio-Environmental Systems Modelling, 4, 18155-18155, 2022.

Ju, W., Gao, P., Wang, J., Zhou, Y., and Zhang, X.: Combining an ecological model with remote sensing and GIS techniques to monitor soil water content of croplands with a monsoon climate, Agricultural Water Management, 97, 1221-1231, 2010.

Ju, W., Chen, J. M., Black, T. A., Barr, A. G., Liu, J., and Chen, B.: Modelling multi-year coupled carbon and water fluxes in a boreal aspen forest, Agricultural and Forest Meteorology, 140, 136-151, 2006.

Kattge, J., Knorr, W., Raddatz, T., and Wirth, C.: Quantifying photosynthetic capacity and its relationship to leaf nitrogen content for global-scale terrestrial biosphere models, Global Change Biology, 15, 976-991, 2009.

Kesselmeier, J., Teusch, N., and Kuhn, U.: Controlling variables for the uptake of atmospheric carbonyl sulfide by soil, Journal of Geophysical Research: Atmospheres, 104, 11577-11584, 1999.

Koffi, E., Rayner, P., Norton, A., Frankenberg, C., and Scholze, M.: Investigating the usefulness of satellite-derived fluorescence data in inferring gross primary productivity within the carbon cycle data assimilation system, Biogeosciences, 12, 4067-4084, 2015.

Kohonen, K.-M., Dewar, R., Tramontana, G., Mauranen, A., Kolari, P., Kooijmans, L. M., Papale, D., Vesala, T., and Mammarella, I.: Intercomparison of methods to estimate gross primary production based on CO 2 and COS flux measurements, Biogeosciences, 19, 4067-4088, 2022.

Kooijmans, L. M., Sun, W., Aalto, J., Erkkilä, K.-M., Maseyk, K., Seibt, U., Vesala, T., Mammarella, I., and Chen, H.: Influences of light and humidity on carbonyl sulfide-based estimates of photosynthesis, Proceedings of the National Academy of Sciences, 116, 2470-2475, 2019.

Kooijmans, L. M. J., Cho, A., Ma, J., Kaushik, A., Haynes, K. D., Baker, I., Luijkx, I. T., Groenink, M., Peters, W., Miller, J. B., Berry, J. A., Ogée, J., Meredith, L. K., Sun, W., Kohonen, K. M., Vesala, T., Mammarella, I., Chen, H., Spielmann, F. M., Wohlfahrt, G., Berkelhammer, M., Whelan, M. E., Maseyk, K., Seibt, U., Commane, R., Wehr, R., and Krol, M.: Evaluation of carbonyl sulfide biosphere exchange in the Simple Biosphere Model (SiB4), Biogeosciences, 18, 6547-6565, 10.5194/bg-18-6547-2021, 2021.

Launois, T., Peylin, P., Belviso, S., and Poulter, B.: A new model of the global biogeochemical cycle of carbonyl sulfide–Part 2: Use of carbonyl sulfide to constrain gross primary productivity in current vegetation models, Atmospheric Chemistry and Physics, 15, 9285-9312, 2015.

https://doi.org/10.5194/egusphere-2023-3032
Preprint. Discussion started: 22 January 2024

Liu, J., Chen, J., Cihlar, J., and Park, W.: A process-based boreal ecosystem productivity simulator using remote sensing inputs, Remote sensing of environment, 62, 158-175, 1997.

Liu, Y., Liu, R., and Chen, J. M.: Retrospective retrieval of long-term consistent global leaf area index (1981–2011) from combined AVHRR and MODIS data, Journal of Geophysical Research: Biogeosciences, 117, 2012.

Liu, Y., Xiao, J., Ju, W., Zhou, Y., Wang, S., and Wu, X.: Water use efficiency of China's terrestrial ecosystems and responses to drought, Scientific reports, 5, 13799, 2015.

Liu, Z., Zhou, Y., Ju, W., and Gao, P.: Simulation of soil water content in farm lands with the BEPS ecological model, Transactions of the Chinese Society of Agricultural Engineering, 27, 67-72, 2011.

Lu, X., Wang, Y.-P., Ziehn, T., and Dai, Y.: An efficient method for global parameter sensitivity analysis and its applications to the Australian community land surface model (CABLE), Agricultural and forest meteorology, 182, 292-303, 2013.

Lu, X., Croft, H., Chen, J. M., Luo, Y., and Ju, W.: Estimating photosynthetic capacity from optimized Rubisco–chlorophyll relationships among vegetation types and under global change, Environmental Research Letters, 17, 014028, 2022.

Luo, Y.: Terrestrial carbon–cycle feedback to climate warming, Annu. Rev. Ecol. Evol. Syst., 38, 683-712, 2007.

MacBean, N., Bacour, C., Raoult, N., Bastrikov, V., Koffi, E., Kuppel, S., Maignan, F., Ottlé, C., Peaucelle, M., and Santaren, D.: Quantifying and reducing uncertainty in global carbon cycle predictions: Lessons and perspectives from 15 years of data assimilation studies with the ORCHIDEE terrestrial biosphere model, Global Biogeochemical Cycles, 36, e2021GB007177, 2022.

Maignan, F., Abadie, C., Remaud, M., Kooijmans, L. M., Kohonen, K.-M., Commane, R., Wehr, R., Campbell, J. E., Belviso, S., and Montzka, S. A.: Carbonyl sulfide: comparing a mechanistic representation of the vegetation uptake in a land surface model and the leaf relative uptake approach, Biogeosciences, 18, 2917-2955, 2021.

Maseyk, K., Berry, J. A., Billesbach, D., Campbell, J. E., Torn, M. S., Zahniser, M., and Seibt, U.: Sources and sinks of carbonyl sulfide in an agricultural field in the Southern Great Plains, Proceedings of the National Academy of Sciences, 111, 9064-9069, 2014.

Medlyn, B. E., Badeck, F. W., De Pury, D., Barton, C., Broadmeadow, M., Ceulemans, R., De Angelis, P., Forstreuter, M., Jach, M., and Kellomäki, S.: Effects of elevated [CO2] on photosynthesis in European forest species: a meta-analysis of model parameters, Plant, Cell & Environment, 22, 1475-1495, 1999.

Miner, G. L., Bauerle, W. L., and Baldocchi, D. D.: Estimating the sensitivity of stomatal conductance to photosynthesis: a review, Plant, Cell & Environment, 40, 1214-1238, 2017.

Mo, X., Chen, J. M., Ju, W., and Black, T. A.: Optimization of ecosystem model parameters through assimilating eddy covariance flux data with an ensemble Kalman filter, Ecological modelling, 217, 157-173, 2008.

Moradkhani, H., Hsu, K. L., Gupta, H., and Sorooshian, S.: Uncertainty assessment of hydrologic model states and parameters: Sequential data assimilation using the particle filter, Water resources research, 41, 2005.

Mu, X. and Chen, Y.: The physiological response of photosynthesis to nitrogen deficiency, Plant Physiology and Biochemistry, 158, 76-82, 2021.

Ogée, J., Sauze, J., Kesselmeier, J., Genty, B., Van Diest, H., Launois, T., and Wingate, L.: A new mechanistic framework to predict OCS fluxes from soils, Biogeosciences, 13, 2221-2240, 2016.

Plischke, E., Borgonovo, E., and Smith, C. L.: Global sensitivity measures from given data, European Journal of Operational Research, 226, 536-550, 2013.

Protoschill-Krebs, G., Wilhelm, C., and Kesselmeier, J.: Consumption of carbonyl sulphide (COS) by higher plant carbonic anhydrase (CA), Atmospheric Environment, 30, 3151-3156, 1996.

Raines, C. A.: The Calvin cycle revisited, Photosynthesis research, 75, 1-10, 2003.

Rastogi, B., Berkelhammer, M., Wharton, S., Whelan, M. E., Itter, M. S., Leen, J. B., Gupta, M. X., Noone, D., and Still, C. J.: Large uptake of atmospheric OCS observed at a moist old growth forest: Controls and implications for carbon cycle applications, Journal of Geophysical Research: Biogeosciences, 123, 3424-3438, 2018.

Reichstein, M., Falge, E., Baldocchi, D., Papale, D., Aubinet, M., Berbigier, P., Bernhofer, C., Buchmann, N., Gilmanov, T., and Granier, A.: On the separation of net ecosystem exchange into assimilation and ecosystem respiration: review and improved algorithm, Global change biology, 11, 1424-1439, 2005.

Rogers, A.: The use and misuse of V c, max in Earth System Models, Photosynthesis research, 119, 15-29, 2014.

https://doi.org/10.5194/egusphere-2023-3032
Preprint. Discussion started: 22 January 2024

Rogers, A., Medlyn, B. E., Dukes, J. S., Bonan, G., Von Caemmerer, S., Dietze, M. C., Kattge, J., Leakey, A. D., Mercado, L. M., and Niinemets, Ü.: A roadmap for improving the representation of photosynthesis in Earth system models, New Phytologist, 213, 22-42, 2017.

Sage, R. F. and Pearcy, R. W.: The nitrogen use efficiency of C3 and C4 plants: II. Leaf nitrogen effects on the gas exchange characteristics of Chenopodium album (L.) and Amaranthus retroflexus (L.), Plant physiology, 84, 959-963, 1987.

Sandoval-Soto, L., Stanimirov, M., Von Hobe, M., Schmitt, V., Valdes, J., Wild, A., and Kesselmeier, J.: Global uptake of carbonyl sulfide (COS) by terrestrial vegetation: Estimates corrected by deposition velocities normalized to the uptake of carbon dioxide (CO 2), Biogeosciences, 2, 125-132, 2005.

Sargsyan, K., Safta, C., Najm, H. N., Debusschere, B. J., Ricciuto, D., and Thornton, P.: Dimensionality reduction for complex models via Bayesian compressive sensing, International Journal for Uncertainty Quantification, 4, 2014.

Schwalm, C. R., Williams, C. A., Schaefer, K., Anderson, R., Arain, M. A., Baker, I., Barr, A., Black, T. A., Chen, G., and Chen, J. M.: A model-data intercomparison of CO2 exchange across North America: Results from the North American Carbon Program site synthesis, Journal of Geophysical Research: Biogeosciences, 115, 2010.

Seibt, U., Kesselmeier, J., Sandoval-Soto, L., Kuhn, U., and Berry, J.: A kinetic analysis of leaf uptake of COS and its relation to transpiration, photosynthesis and carbon isotope fractionation, Biogeosciences, 7, 333-341, 2010.

Spielmann, F., Wohlfahrt, G., Hammerle, A., Kitz, F., Migliavacca, M., Alberti, G., Ibrom, A., El-Madany, T. S., Gerdel, K., and Moreno, G.: Gross primary productivity of four European ecosystems constrained by joint CO2 and COS flux measurements, Geophysical research letters, 46, 5284-5293, 2019.

Staudt, K., Falge, E., Pyles, R. D., Paw U, K. T., and Foken, T.: Sensitivity and predictive uncertainty of the ACASA model at a spruce forest site, Biogeosciences, 7, 3685-3705, 2010.

Stimler, K., Montzka, S. A., Berry, J. A., Rudich, Y., and Yakir, D.: Relationships between carbonyl sulfide (COS) and CO2 during leaf gas exchange, New Phytologist, 186, 869-878, 2010.

Sun, W., Berry, J. A., Yakir, D., and Seibt, U.: Leaf relative uptake of carbonyl sulfide to CO2 seen through the lens of stomatal conductance–photosynthesis coupling, New Phytologist, 235, 1729-1742, 2022.

Sun, W., Maseyk, K., Lett, C., and Seibt, U.: A soil diffusion–reaction model for surface COS flux: COSSM v1, Geoscientific Model Development, 8, 3055-3070, 2015.

Tang, J. and Zhuang, Q.: A global sensitivity analysis and Bayesian inference framework for improving the parameter estimation and prediction of a process-based Terrestrial Ecosystem Model, Journal of Geophysical Research: Atmospheres, 114, 2009.

Tonkin, M. and Doherty, J.: Calibration-constrained Monte Carlo analysis of highly parameterized models using subspace techniques, Water Resources Research, 45, 2009.

Vesala, T., Kohonen, K.-M., Kooijmans, L. M., Praplan, A. P., Foltýnová, L., Kolari, P., Kulmala, M., Bäck, J., Nelson, D., and Yakir, D.: Long-term fluxes of carbonyl sulfide and their seasonality and interannual variability in a boreal forest, Atmospheric Chemistry and Physics, 22, 2569-2584, 2022.

Wang, J., Jiang, F., Wang, H., Qiu, B., Wu, M., He, W., Ju, W., Zhang, Y., Chen, J. M., and Zhou, Y.: Constraining global terrestrial gross primary productivity in a global carbon assimilation system with OCO-2 chlorophyll fluorescence data, Agricultural and Forest Meteorology, 304, 108424, 2021.

Wehr, R., Commane, R., Munger, J. W., McManus, J. B., Nelson, D. D., Zahniser, M. S., Saleska, S. R., and Wofsy, S. C.: Dynamics of canopy stomatal conductance, transpiration, and evaporation in a temperate deciduous forest, validated by carbonyl sulfide uptake, Biogeosciences, 14, 389-401, 2017.

Whelan, M. E., Hilton, T. W., Berry, J. A., Berkelhammer, M., Desai, A. R., and Campbell, J. E.: Carbonyl sulfide exchange in soils for better estimates of ecosystem carbon uptake, Atmospheric Chemistry and Physics, 16, 3711-3726, 2016.

Whelan, M. E., Shi, M., Sun, W., Vries, L. K. d., Seibt, U., and Maseyk, K.: Soil carbonyl sulfide (OCS) fluxes in terrestrial ecosystems: an empirical model, Journal of Geophysical Research: Biogeosciences, 127, e2022JG006858, 2022.

Whelan, M. E., Lennartz, S. T., Gimeno, T. E., Wehr, R., Wohlfahrt, G., Wang, Y., Kooijmans, L. M., Hilton, T. W., Belviso, S., and Peylin, P.: Reviews and syntheses: Carbonyl sulfide as a multi-scale tracer for carbon and water cycles, Biogeosciences, 15, 3625-3657, 2018.

Wohlfahrt, G., Brilli, F., Hörtnagl, L., Xu, X., Bingemer, H., Hansel, A., and Loreto, F.: Carbonyl sulfide (COS) as a tracer for canopy photosynthesis, transpiration and stomatal conductance: potential and limitations, Plant, cell & environment, 35, 657-667, 2012.

https://doi.org/10.5194/egusphere-2023-3032
Preprint. Discussion started: 22 January 2024

Woodward, F. I., Smith, T. M., and Emanuel, W. R.: A global land primary productivity and phytogeography model, Global biogeochemical cycles, 9, 471-490, 1995.

Wu, M., Ran, Y., Jansson, P.-E., Chen, P., Tan, X., and Zhang, W.: Global parameters sensitivity analysis of modeling water, energy and carbon exchange of an arid agricultural ecosystem, Agricultural and Forest Meteorology, 271, 295-306, 2019.

Wu, M., Tan, X., Wu, J., Huang, J., Jansson, P.-E., and Zhang, W.: Coupled water transport and heat flux in seasonally frozen soils: uncertainties identification in multi-site calibration, Environmental Earth Sciences, 79, 524, 2020.

Xiao, Z., Liang, S., Wang, J., Xiang, Y., Zhao, X., and Song, J.: Long-time-series global land surface satellite leaf area index product derived from MODIS and AVHRR surface reflectance, IEEE Transactions on Geoscience and Remote Sensing, 54, 5301-5318, 2016.

Xing, X., Wu, M., Zhang, W., Ju, W., Tagesson, T., He, W., Wang, S., Wang, J., Hu, L., and Yuan, S.: Modeling China's terrestrial ecosystem gross primary productivity with BEPS model: Parameter sensitivity analysis and model calibration, Agricultural and Forest Meteorology, 343, 109789, 2023.

Yang, F., Qubaja, R., Tatarinov, F., Rotenberg, E., and Yakir, D.: Assessing canopy performance using carbonyl sulfide measurements, Global Change Biology, 24, 3486-3498, 2018.

Yi, D. H., Kim, D. W., and Park, C. S.: Parameter identifiability in Bayesian inference for building energy models, Energy and Buildings, 198, 318-328, 2019.

Yuan, W., Liu, S., Zhou, G., Zhou, G., Tieszen, L. L., Baldocchi, D., Bernhofer, C., Gholz, H., Goldstein, A. H., and Goulden, M. L.: Deriving a light use efficiency model from eddy covariance flux data for predicting daily gross primary production across biomes, Agricultural and Forest Meteorology, 143, 189-207, 2007.

Zaehle, S., Sitch, S., Smith, B., and Hatterman, F.: Effects of parameter uncertainties on the modeling of terrestrial biosphere dynamics, Global Biogeochemical Cycles, 19, 2005.

Zierl, B.: A water balance model to simulate drought in forested ecosystems and its application to the entire forested area in Switzerland, Journal of Hydrology, 242, 115-136, 2001.